

EmoTalkingGaussian: Continuous Emotion-conditioned Talking Head Synthesis

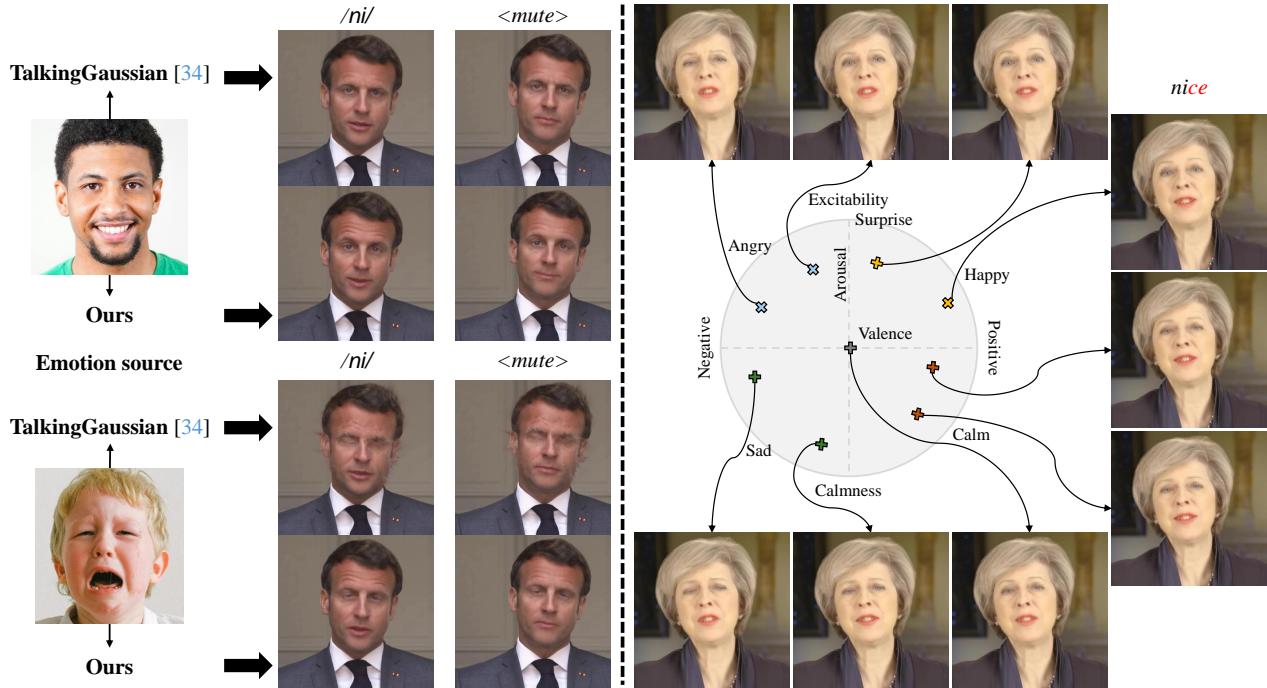
Junuk Cha^{1,2,†}Seongro Yoon²Valeriya Strizhkova²Francois Bremond²Seungryul Baek¹¹UNIST²Inria

Figure 1. The state-of-the-art 3D talking head synthesis method, TalkingGaussian [37], manipulates expressions based on action units [19]; however, its ability to express diverse emotions is limited, and the image quality becomes inferior when representing unseen emotional expression of the emotion source image [1]. Our method can reflect diverse expressions and emotions based on action units as well as valence/arousal [53], and it renders the talking head with lip shape well-aligned to the input audio (*/ni/* and *<mute>*), as shown in the left panel. The right panel demonstrates our method’s capability to convey continuous emotions through valence/arousal adjustments, while keeping the lip synchronized to the audio. The “ce” in “nice,” which the speaker is pronouncing, is highlighted in red.

Abstract

3D Gaussian splatting-based talking head synthesis has recently gained attention for its ability to render high-fidelity images with real-time inference speed. However, since it is typically trained on only a short video that lacks the diversity in facial emotions, the resultant talking heads struggle to represent a wide range of emotions. To address this issue, we propose a lip-aligned emotional face generator and leverage it to train our EmoTalkingGaussian model. It is able to manipulate facial emotions conditioned on continuous emotion values (i.e., valence and arousal); while retaining synchronization of lip

movements with input audio. Additionally, to achieve the accurate lip synchronization for in-the-wild audio, we introduce a self-supervised learning method that leverages a text-to-speech network and a visual-audio synchronization network. We experiment our EmoTalkingGaussian on publicly available videos and have obtained better results than state-of-the-arts in terms of image quality (measured in PSNR, SSIM, LPIPS), emotion expression (measured in V-RMSE, A-RMSE, V-SA, A-SA, Emotion Accuracy), and lip synchronization (measured in LMD, Sync-E, Sync-C), respectively.

† This research was conducted when Junuk Cha was an intern at Inria.

1. Introduction

3D Gaussian splatting (3DGS) [30] has been recently established as the alternative to neural radiance fields (NeRF) [40], offering substantial improvements in both rendering speed and quality. Talking head synthesis domain also reflects the trend: NeRF-based approaches [9, 21, 36, 48, 54, 59, 67] have been prevailed; while they are being rapidly replaced by the 3D Gaussian splatting-based approaches [12, 24, 37, 69], thanks to its real-time speed and high-fidelity rendering quality.

Despite the advancements, we argue that existing pipelines lack the important aspect of human *emotions*. We observed that existing models [12, 37] are able to handle basic facial expressions such as *eye blinking* and *eyebrow movement*, as seen in the 3-5 minute training video; however they struggle to represent continuous and diverse emotions such as *happy*, *sad*, *angry*, etc. When talking, humans convey diverse emotions. To achieve the truly life-like talking heads by filling the gap, we insist that synthesized talking heads need to represent such diverse human emotions while talking. Although He *et al.* [24] proposed a method that relies on collecting new data, a significant drawback is the high cost involved, as additional data must be captured to train a 3D Gaussian model for each new person.

In this paper, we propose EmoTalkingGaussian that integrates continuous emotional expression into 3D Gaussian splatting-based talking head synthesis. To manipulate facial emotions, we utilize valence and arousal [53] as conditions of EmoTalkingGaussian. Valence represents the degree of positiveness or negativeness, and arousal indicates the level of excitability or calmness, both ranging from -1 to 1. Unlike action units [19] that capture basic facial expressions such as *eye blinking*, valence and arousal enable continuous adjustments to facial emotions, (e.g., *happy*, *surprise*, *sad*, etc), as shown in Fig. 1. To train EmoTalkingGaussian on diverse emotional facial images not seen in the original train video, one solution is to augment the data using EmoStyle [4], which modifies the emotion of a source image based on valence/arousal inputs. However, when training EmoTalkingGaussian with data obtained from the pre-trained EmoStyle, a mismatch arises between lip movements and speech audio, as EmoStyle does not handle their alignment, as shown in Fig. 2. To resolve this, we propose a lip-aligned emotional face generator to better align the lip movements with the source image while effectively reflecting the intended emotions based on valence/arousal. Furthermore, to mitigate the domain gap between real images and synthetic images generated by our lip-aligned emotional face generator, we apply a loss function that leverages normal maps generated by [3]. To improve the synchronization of lip movements with in-the-wild audio samples, we use a text-to-speech network [18] to generate curated speech audio data that is small but diverse in English pronunciation. By incorporating SyncNet [14], we apply a loss function that encourages the alignment between input audio and the image rendered by EmoTalkingGaussian, improving synchronization.

The main contributions are summarized as follows:

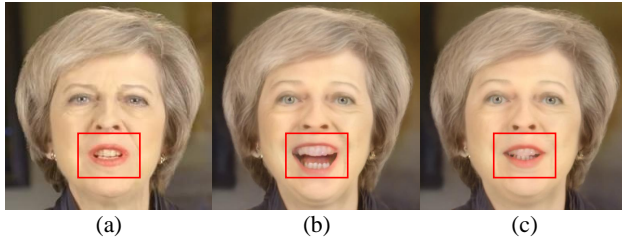


Figure 2. (a) shows the source image, (b) and (c) represent images for the ‘*happy&surprise*’ emotion (valence of 0.8, arousal of 0.6), which are generated by EmoStyle [4] and our lip-aligned emotional face generator, respectively.

- We propose EmoTalkingGaussian, an audio-driven talking head generation model that leverages valence and arousal to render continuous emotional expressions without requiring additional data capturing.
- We introduce self-supervised learning with a sync loss to improve lip synchronization, utilizing a curated speech audio dataset generated via a text-to-speech network.
- Extensive experiments demonstrate that EmoTalkingGaussian effectively renders diverse emotional talking head with lip movements synchronized to the input audio, surpassing the limitations in emotional expressiveness of existing state-of-the-art methods.

2. Related Work

2.1. 3D Gaussian Splatting

3D Gaussian Splatting (3DGS) [30] was proposed to address the high computational cost and slow rendering speed issues faced by NeRF [40]. 3DGS enables fast and efficient rendering, making it highly suitable for real-time applications. 3DGS represents scenes using point-based 3D Gaussians, where each Gaussian contains attributes such as position, scale, rotation, color, and opacity. These Gaussians are aggregated and rendered efficiently using fast differentiable rasterization. In addition to its rendering speed, 3DGS maintains high visual quality, producing detailed and accurate representations of complex scenes, making it suitable for high-fidelity rendering tasks. Thanks to its efficiency and high fidelity, recent research has extended to complex 3D representations of humans [26, 27, 37, 42, 44, 50, 76], demonstrating potential for diverse applications.

2.2. Emotional Face Synthesis

Some emotional face synthesis approaches use Conditional GANs [41], which are conditioned on either a one-hot encoding vector [16] or a continuous emotion vector [15, 39]. Lindt *et al.* [39] take valence and arousal values as input to generate corresponding face images. However, they mentioned that preserving the identity becomes difficult if the input image expresses the extreme emotion. Ding *et al.* [15] update valence and arousal vectors so that the generated images are classified as desired emotions. Some methods [32, 52] employ StarGAN [13] to manipu-

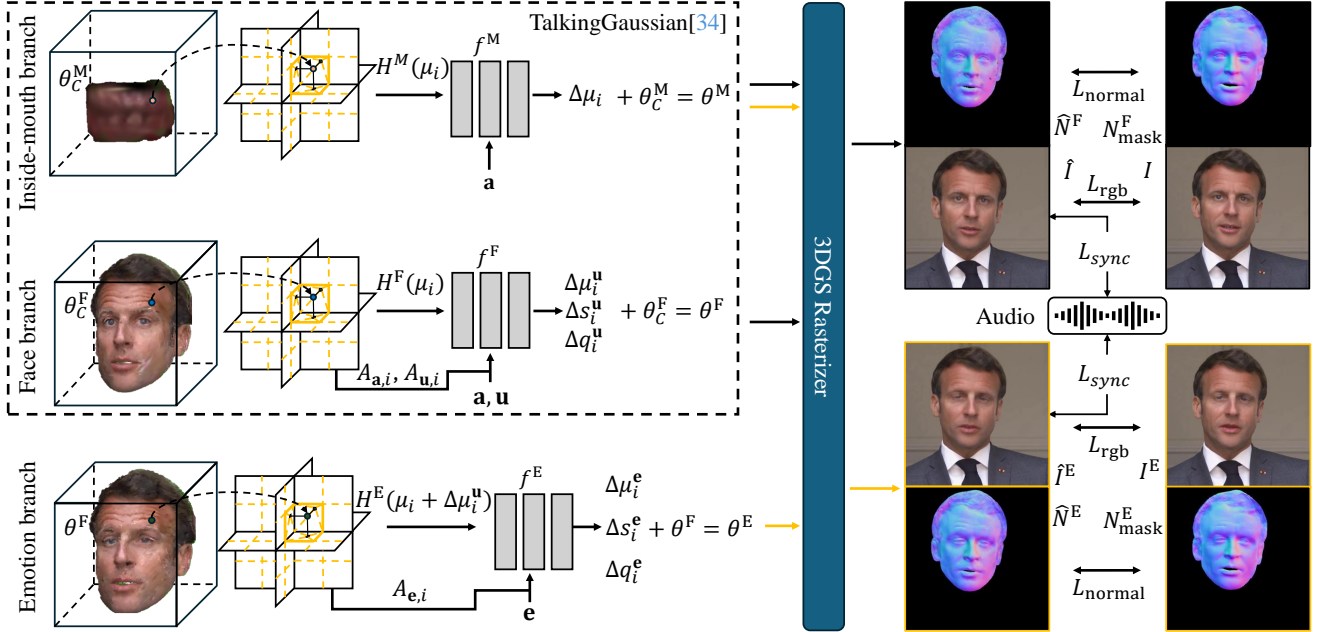


Figure 3. Overview of the EmoTalkingGaussian: Our EmoTalkingGaussian is composed of three branches. First, the inside-mouth branch estimates the position offsets of 3D Gaussians based on audio features \mathbf{a} . Second, the face branch estimates the position, scaling factor, and quaternion offsets based on audio features \mathbf{a} and action units \mathbf{u} . Our inside-mouth branch and face branch are inherited from TalkingGaussian [37], indicated by the dashed rectangle. Finally, the third branch, the emotion branch, estimates the position, scaling factor, and quaternion offsets based on emotion inputs \mathbf{e} (valence/arousal). We render the mouth region and face region \hat{I} along the black arrow. Then, we render the mouth region and emotional face region \hat{I}^E along the yellow arrow. We apply RGB loss, normal loss, along with audio and lip synchronization loss to improve visual fidelity and overall alignment.

late the emotion in the input image. Pumarola *et al.* [52] use action units (AUs) to control face muscles, while Kollias *et al.* [32] use valence and arousal values to control the emotions of the generated images. StyleGAN [13] and StyleGAN2 [29] are utilized in several approaches [2, 4, 23, 31, 47, 55]. EmoStyle [4] uses valence and arousal values to control facial emotions and it proposed a combination of multiple losses related to pixel, landmark, identity, and emotion. Diffusion [25, 56] mechanism-based methods utilize the 3D face mesh model, FLAME [38], to create surface normals, albedo, and Lambertian renderings for conditioning [17]. These methods [45, 46] extend the valence and arousal space into 3D to express more diverse emotions or employ ID vectors to generate desired facial identities.

2.3. Audio-driven Talking Head Synthesis

2D-based talking head synthesis approaches [10, 14, 20, 51, 57, 63, 73, 75] have advanced by utilizing intermediate representations such as motion [11, 64, 65] and landmarks [70, 74, 74, 77]. However, these 2D-based methods struggle to maintain naturalness and consistency, especially when there are large changes in head pose.

3D-based talking head synthesis methods [12, 21, 35, 36, 54, 60, 67] utilize neural radiance fields [40] (NeRF) or 3D Gaussians splatting [30] (3DGS) to generate a photo-realistic and personalized head models. Recently, TalkingGaussian [37] proposed the 3DGS-based method for audio-driven talking

head synthesis. It employs audio features to synchronize the lips with the input audio and utilizes the action units (AUs) to manipulate facial expressions. However, because it is trained on only a 3-5 minute video, it struggles to represent a continuous and wide range of emotions. This limitation is not exclusive to TalkingGaussian but is a common issue among 3D-based approaches. To address this issue, He *et al.* [24] collected EmoTalk3D dataset and proposed *Speech-to-Geometry-to-Appearance* framework. However, because this method is data-driven and person-specific, it has the drawback of requiring data collection for new individuals.

3. Method

We propose EmoTalkingGaussian, which renders emotional talking heads using 3D Gaussian splatting method, conditioned on valence/arousal values, action units, and audio input: We first employ TalkingGaussian [37] pipeline to synthesize 3D Gaussian splatting-based talking heads conditioned on audio and action units. Then, we generate lip-aligned emotional face images to effectively train the emotion manipulator of EmoTalkingGaussian with diverse emotional facial images. This simple method leads us to synthesize talking heads reflecting diverse valence/arousal conditions, though the rendering quality slightly diminishes. Furthermore, the lip becomes unsynchronized specifically when conditioned on unseen audio. To relieve the challenges, we improve rendering quality by involving a

normal map loss and enhance lip synchronization by employing a sync loss which enforces consistency between the image rendered by EmoTalkingGaussian and the input audio generated by a text-to-speech network [18]. Our EmoTalkingGaussian framework is shown in Fig. 3.

3.1. 3D Gaussian Splatting

3D Gaussian splatting [30] utilizes a set of 3D Gaussians, which are represented by a position μ , a scaling factor s , a rotation quaternion q , an opacity value α , and a color c , to describe a 3D scene. In the point-based rendering, at pixel \mathbf{x}_p , the color $C(\mathbf{x}_p)$ and the opacity $\mathcal{A}(\mathbf{x}_p)$ are calculated based on the contributions of a set of N Gaussians as follows:

$$C(\mathbf{x}_p) = \sum_{i \in N} c_i \tilde{\alpha}_i \prod_{j=1}^{i-1} (1 - \tilde{\alpha}_j), \quad (1)$$

$$\mathcal{A}(\mathbf{x}_p) = \sum_{i \in N} \tilde{\alpha}_i \prod_{j=1}^{i-1} (1 - \tilde{\alpha}_j), \quad (2)$$

where $\tilde{\alpha}_i = \alpha_i \mathcal{G}_i^{proj}(\mathbf{x}_p)$, $\mathcal{G}_i(\mathbf{x}) = e^{-\frac{1}{2}(\mathbf{x} - \mu_i)^T \Sigma_i^{-1} (\mathbf{x} - \mu_i)}$. A covariance matrix Σ_i is derived from s_i and q_i , and a 2D Gaussian \mathcal{G}_i^{proj} is the projection of a 3D Gaussian \mathcal{G}_i onto the image plane. During optimization, 3DGS updates parameters $\theta = \{\mu, s, q, \alpha, c\}$, and applies both densification and pruning of the 3D Gaussians to find the appropriate number of Gaussians for accurately representing the scene.

Following GaussianShader [28], which proposed a method for rendering normal maps directly from 3D Gaussians, we add a normal residual $\Delta \mathbf{n}$ to the 3D Gaussian parameters for the face region, defined as $\theta = \{\mu, s, q, \alpha, c, \Delta \mathbf{n}\}$. This residual refines the normal direction to improve the quality of the rendered normal maps. We then use the rendered normal map to apply the normal map loss.

3.2. EmoTalkingGaussian

We propose the EmoTalkingGaussian that synthesizes talking heads conditioned on the input audio as well as the continuous emotion and expression values, i.e., valence/arousal and action units. We employ TalkingGaussian [37] pipeline as our baseline architecture for synthesizing the talking head. It separately models an inside-mouth region and a face region using two distinct persistent Gaussian fields. These fields remain stable and preserve the geometry of the face while allowing dynamic deformations based on input audio features \mathbf{a} extracted by DeepSpeech [22] and upper-face action units \mathbf{u} extracted by OpenFace [6]. To enable precise control over the deformation of the Gaussians, offsets are calculated using a tri-plane hash encoder H [36], which allows accurate adjustments to the Gaussians' parameters.

For the inside-mouth region, the offset $\delta_i^m = \{\Delta \mu_i\}$ is estimated via the inside-mouth region manipulation network

f^M conditioned only on \mathbf{a} as follows:

$$\delta_i^m = f^M(H^M(\mu_i) \oplus \mathbf{a}), \quad (3)$$

where μ_i denotes the position of the canonical Gaussian θ_C^M , and $H^M(\cdot)$ is the tri-plane hash encoder for the inside-mouth. The inside-mouth deformed Gaussians are represented as: $\theta^M = \theta_C^M + \delta^m = \{\mu + \Delta \mu, s, q, \alpha, c\}$

For the face region, the offset $\delta_i^u = \{\Delta \mu_i^u, \Delta s_i^u, \Delta q_i^u\}$ for each Gaussian is estimated using both \mathbf{a} and \mathbf{u} through the face region manipulation network f^F as follows:

$$\delta_i^u = f^F(H^F(\mu_i) \oplus \mathbf{a}_{r,i} \oplus \mathbf{u}_{r,i}), \quad (4)$$

where $\mathbf{a}_{r,i} = A_{\mathbf{a},i} \odot \mathbf{a}$ and $\mathbf{u}_{r,i} = A_{\mathbf{u},i} \odot \mathbf{u}$ represent the region-aware features at position μ_i , and the attention maps $A_{\mathbf{a},i}$ and $A_{\mathbf{u},i}$ are derived from \mathbf{a} and \mathbf{u} , respectively. \odot and \oplus denote Hadamard product and concatenation, respectively. μ_i is the position of the canonical Gaussian θ_C^F , and $H^F(\cdot)$ is the tri-plane hash encoder for the face. The face deformed Gaussians are represented as: $\theta^F = \theta_C^F + \delta^u = \{\mu + \Delta \mu^u, s + \Delta s^u, q + \Delta q^u, \alpha, c, \Delta \mathbf{n}\}$.

We introduce the emotion branch to manipulate the facial emotion based on continuous valence and arousal values \mathbf{e} . This allows the emotion manipulation network f^E to estimate the offset $\delta_i^e = \{\Delta \mu_i^e, \Delta s_i^e, \Delta q_i^e\}$ that aligns with the desired emotion.

$$\delta_i^e = f^E(H^E(\mu_i + \Delta \mu_i^u) \oplus \mathbf{e}_{r,i}), \quad (5)$$

where $\mathbf{e}_{r,i} = A_{\mathbf{e},i} \odot \mathbf{e}$ represents the region-aware features at position $\mu_i + \Delta \mu_i^u$ of the deformed Gaussian θ^F , and $H^E(\cdot)$ is the tri-plane hash encoder for the emotion. The attention map $A_{\mathbf{e},i}$ is derived from \mathbf{e} , and \odot and \oplus denote Hadamard product and concatenation, respectively. The emotional deformed Gaussians are expressed as: $\theta^E = \theta^F + \delta^e = \{\mu + \Delta \mu^u + \Delta \mu^e, s + \Delta s^u + \Delta s^e, q + \Delta q^u + \Delta q^e, \alpha, c, \Delta \mathbf{n}\}$.

3.3. Synthetic Image and Audio Augmentation

When training the EmoTalkingGaussian using the provided personal speech video, the emotion manipulation network f^E is not able to properly model the emotions for given subjects. Furthermore, the speech audio data is also limited. To relieve the challenges of properly training f^E , the face region manipulation network f^F and the inside-mouth region manipulation f^M with rich emotional and speech variations, we involve the synthetic images and audio. Especially, we augment the subject-specific emotional face image by involving a lip-aligned emotional face generator. Also, we use the text-to-speech network [18] to synthesize new speech audio.

3.3.1 Lip-aligned Emotional Face Generator

To obtain the lip-aligned emotional face generation network g^{LEF} , we initially adopt the framework of EmoStyle [4] that is able to adjust the facial emotions in an input image I

conditioned on the valence and arousal \mathbf{e} , while preserving background, identity and head pose. However, during the adjustment, EmoStyle [4] also transforms lips to excessively represent the emotions.

To prevent this, we extend EmoStyle [4] to be additionally conditioned on the lip landmarks of I , ensuring that the lip shape on the generated image closely matches that of I . We extract lip heatmaps H from I using the off-the-shelf landmark detector D_l [7]. The heatmaps H are then processed by a 2D convolutional encoder E , which outputs a lip embedding vector z_l . We concatenate the lip embedding vector z_l with an emotional latent code \mathcal{W}' generated by the original EmoStyle. We then introduce the LipExtract module M_{lip} to further process the combined embedding. The LipExtract module outputs a lip modification vector d_l , which is added to \mathcal{W}' , resulting in a lip-aligned emotional latent code \mathcal{W}'' . This process is expressed as follows:

$$\begin{aligned} \mathcal{W}'' &= \mathcal{W}' + d_l, \quad d_l = M_{\text{lip}}(z_l \oplus \mathcal{W}'), \\ \mathcal{W}' &= \text{EmoStyle}(I), \quad z_l = E(H), \quad H = D_l(I), \end{aligned} \quad (6)$$

where \oplus means concatenation. StyleGAN2 [29] uses \mathcal{W}'' to generate the synthetic emotional image I^E , aligning the lips with those in I while expressing the desired emotion.

We utilize the following loss functions to train the encoder E and the LipExtract module M_{lip} , and fine-tune the StyleGAN2 [29], while freezing other components of Emostyle [4]:

$$\mathcal{L} = \lambda_1 \cdot \mathcal{L}_{ll} + \lambda_2 \cdot \mathcal{L}_{lp} + \lambda_3 \cdot \mathcal{L}_{reg} + \lambda_4 \cdot \mathcal{L}_{emo} + \lambda_5 \cdot \mathcal{L}_{id}, \quad (7)$$

where lip landmark loss \mathcal{L}_{ll} , lip pixel loss \mathcal{L}_{lp} , and regularization loss \mathcal{L}_{reg} are defined as follows:

$$\mathcal{L}_{ll} = \|\hat{L}_l - L_l\|_2^2, \quad \mathcal{L}_{lp} = \|\mathbb{M}_l \odot (I^E - I)\|_2^2, \quad \mathcal{L}_{reg} = \|d_l\|_2^2, \quad (8)$$

where L_l and \hat{L}_l represent the lip landmarks estimated from the input image I and the output image I^E using the landmark detector [7], respectively. \mathbb{M}_l denotes a rectangle mask created from the lip landmarks L_l . The losses \mathcal{L}_{ll} and \mathcal{L}_{lp} ensure that the lips in I and I^E are aligned. The regularization loss \mathcal{L}_{reg} prevents d_l from diverging. Additionally, the emotion loss \mathcal{L}_{emo} [4] guarantees that I^E reflects the desired emotion, while the identity loss \mathcal{L}_{id} [4] ensures that I^E preserves the identity of I . λ_i is the weight of each loss term.

3.3.2 TTS-based Speech Audio Generator

To enhance the generalizability of lip sync, we employ ChatGPT [43] and a text-to-speech algorithm [18] to generate curated speech audio data. Specifically, we prompt ChatGPT to create 10 text samples that cover a broad range of English phonetic variations, including essential phonemes and various pronunciation phenomena. For instance, the sentence ‘‘The quick brown fox jumps over the lazy dog’’ includes most English consonants and vowels, providing comprehensive phoneme coverage.

By converting these texts into speech audio using the text-to-speech network [18], we perform self-supervised learning to train EmoTalkingGaussian on a diverse set of speech variations. To do this, we apply a sync loss $\mathcal{L}_{\text{sync}}$, which calculates the L2 loss between audio features and image features using SyncNet [14] as follows:

$$\mathcal{L}_{\text{sync}} = \|S_I(\hat{I}) - S_A(A)\|_2^2, \quad (9)$$

where S_I and S_A denote the image encoder and audio encoder of SyncNet. A represents the audio input, and \hat{I} denotes the image rendered by EmoTalkingGaussian, conditioned on A . This loss enhances synchronization accuracy, enabling our model to be trained on additional speech audio data without paired RGB video, thus allowing for greater flexibility in data use.

3.4. Training

We independently train each branch of EmoTalkingGaussian (inside-mouth, face, and emotion).

3.4.1 Optimizing Canonical Gaussians

We optimize the inside-mouth canonical Gaussians θ_C^M and the face canonical Gaussians θ_C^F through the L1 loss L_1 and D-SSIM loss $L_{D\text{-SSIM}}$:

$$\mathcal{L}_{\text{rgb}} = \mathcal{L}_1(\hat{I}_C, I_{\text{mask}}) + \gamma_1 \mathcal{L}_{D\text{-SSIM}}(\hat{I}_C, I_{\text{mask}}), \quad (10)$$

where \hat{I}_C represents the image rendered from either θ_C^M or θ_C^F , and I_{mask} denotes the masked ground truth for either the inside-mouth region or the face region, where the mask is extracted from the ground truth I following [37]. For optimizing θ_C^F , the normal map loss is additionally applied to update the positions μ and the normal residuals $\Delta \mathbf{n}$ as follows:

$$\mathcal{L}_{\text{normal}} = \gamma_2 \mathcal{L}_1(\hat{N}_C^F, N_{\text{mask}}^F) + \gamma_3 \mathcal{L}_{\text{tv}}(\hat{N}_C^F) + \gamma_4 \|\Delta \mathbf{n}\|_2^2, \quad (11)$$

where \hat{N}_C^F represents the normal map rendered from 3D Gaussians θ_C^F , while N_{mask}^F is the masked normal map extracted by the predictor [3]. \mathcal{L}_{tv} denotes the total variation loss used to enforce the spatial smoothness in the rendered normal map, and the regularization loss ensures that $\Delta \mathbf{n}$ does not diverge. γ_i is the weight of each loss term.

3.4.2 Training Networks for Inside-Mouth and Face Regions

We train the tri-plane hash encoder H (inside-mouth H^M and face H^F) and manipulation network f (inside-mouth f^M and face f^F) with the following loss function:

$$\mathcal{L} = \mathcal{L}_{\text{rgb}} + \mathcal{L}_{\text{normal}} + \mathcal{L}_{\text{sync}}, \quad (12)$$

Method	PSNR (\uparrow)	SSIM (\uparrow)	LPIPS (\downarrow)	LMD (\downarrow)	Sync-E(\downarrow)/C(\uparrow)	AUE-U(\downarrow)/L(\downarrow)	FPS
Ground truth	-	1	0	0	6.546/7.827	0/0	-
ER-NeRF [36]	33.06	0.935	0.0274	3.110	8.443/5.554	0.779/0.565	34
GaussianTalker [12]	33.02	0.939	0.0333	3.206	8.554/5.741	0.766/0.523	121
TalkingGaussian [37]	33.64	0.940	<u>0.0256</u>	<u>2.610</u>	8.129/5.919	0.279/0.550	<u>108</u>
Ours w/o Emo. branch	33.87	0.944	0.0255	2.557	<u>7.750/6.270</u>	0.207/0.515	107
Ours	<u>33.78</u>	<u>0.943</u>	0.0267	2.638	7.702/6.279	<u>0.278/0.520</u>	101

Table 1. We compare quantitative results for self-reconstruction scenario. We highlight the best results in **bold** and the second-best in underline. ‘‘Ours w/o Emo. branch’’ denotes our method without the emotion branch.

where

$$\begin{aligned} \mathcal{L}_{\text{rgb}} &= \mathcal{L}_1(\hat{I}, I_{\text{mask}}) + \beta_1 \mathcal{L}_{\text{D-SSIM}}(\hat{I}, I_{\text{mask}}) \\ &+ \beta_2 \mathcal{L}_{\text{LPIPS}}(\hat{I}, I_{\text{mask}}), \end{aligned} \quad (13)$$

$$\begin{aligned} \mathcal{L}_{\text{normal}} &= \beta_3 \mathcal{L}_1(\hat{N}^{\text{F}}, N_{\text{mask}}^{\text{F}}) + \beta_4 \mathcal{L}_{\text{tv}}(\hat{N}^{\text{F}}) \\ &+ \beta_5 \|\Delta \mathbf{n}\|_2^2, \end{aligned} \quad (14)$$

where \hat{I} is rendered from either θ^{M} or θ^{F} , and \hat{N}^{F} is rendered from θ^{F} . $\mathcal{L}_{\text{LPIPS}}$ denotes the LPIPS loss. Furthermore, we apply a sync loss $\mathcal{L}_{\text{sync}}$, defined in Eq. 9, using both original and synthesized audio data to improve lip synchronization accuracy. β_i is the weight of each loss term.

3.4.3 Training Network for Emotion

We train the emotion tri-plane hash encoder H^{E} and the emotion manipulation network f^{E} with the following loss function:

$$\mathcal{L} = \mathcal{L}_{\text{rgb}} + \mathcal{L}_{\text{normal}} + \mathcal{L}_{\text{sync}}, \quad (15)$$

where

$$\begin{aligned} \mathcal{L}_{\text{rgb}} &= \mathcal{L}_1(\hat{I}^{\text{E}}, I_{\text{mask}}) + \kappa_1 \mathcal{L}_{\text{D-SSIM}}(\hat{I}^{\text{E}}, I_{\text{mask}}) \\ &+ \kappa_2 \mathcal{L}_{\text{LPIPS}}(\hat{I}^{\text{E}}, I_{\text{mask}}), \end{aligned} \quad (16)$$

$$\begin{aligned} \mathcal{L}_{\text{normal}} &= \kappa_3 \mathcal{L}_1(\hat{N}^{\text{E}}, N_{\text{mask}}^{\text{E}}) + \kappa_4 \mathcal{L}_{\text{tv}}(\hat{N}^{\text{E}}) \\ &+ \kappa_5 \|\Delta \mathbf{n}\|_2^2, \end{aligned} \quad (17)$$

where both \hat{I}^{E} and \hat{N}^{E} are rendered from θ^{E} . Additionally, we apply a sync loss $\mathcal{L}_{\text{sync}}$, defined in Eq. 9, using both original and synthesized audio data to enhance the lip synchronization. κ_i is the weight of each loss term.

4. Experiments

4.1. Setup

Dataset. We evaluate our method on publicly available videos [21, 36, 67], following the setting of Li *et al.* [37]. The dataset has 4 subjects: ‘‘Macron’’, ‘‘Obama’’, ‘‘Lieu’’, and ‘‘May.’’ Each video is cropped and resized to ensure that faces are centered. The average video length is 6,500 at 25 FPS, with a resolution of 512×512 pixels, except for the ‘‘Obama’’ video which has 450×450 resolution. Each video is divided into train and test sets with a 10:1 ratio.

Method	Testset A	Testset B
	Sync-E(\downarrow)/C(\uparrow)	Sync-E(\downarrow)/C(\uparrow)
Ground truth	7.589/7.158	7.398/7.112
ER-NeRF [36]	9.960/4.305	9.397/4.938
GaussianTalk. [12]	10.208/4.375	9.419/5.001
TalkingGau. [37]	9.369/4.835	9.009/5.261
Ours	9.262/4.930	8.746/5.426

Table 2. We evaluate cross-domain audio scenario, highlighting the best results in **bold**.

Baselines. We compare our method with NeRF-based approaches, ER-NeRF [36], and 3DGS-based approaches, TalkingGaussian [37] and GaussianTalker [12]. These baseline methods are limited to basic facial expressions, such as eye blinking, and do not enable manipulation of facial emotions. Some 2D-based talking head generation methods [20, 63] require large datasets for training, therefore we do not include them in our comparisons.

Scenarios. We evaluate methods across three scenarios: *self-reconstruction*, *cross-domain audio*, and *emotion-conditioned* scenarios. In the *self-reconstruction* scenario, we evaluate methods using the test set’s audio, action units, and valence/arousal values. In the *cross-domain audio* scenario, we train models on train set and test them on two cross-domain audio samples extracted from [58], to evaluate their performance on in-the-wild audio. In the *emotion-conditioned* scenario, we evaluate the models’ ability to reflect the desired emotion. For our model, we manipulate emotional expressions by using 12 points selected on a 2D circle as inputs for valence and arousal. For other baseline models, action units are used. Specifically, we generate emotional facial images using EmoStyle [4] with the 12 valence and arousal points, then extract action units from these images to use as input. Additionally, we use the cross-domain audio sample extracted from [58].

Metrics. We utilize PSNR, SSIM [66], and LPIPS [72] to evaluate the quality of the rendered images. To evaluate lip synchronization, we use the mouth landmark distance (LMD) [10], and the synchronization error (Sync-E) and the synchronization confidence score (Sync-C) of SyncNet [14]. We measure the upper-face action unit error (AUE-U) and lower-face action unit error (AUE-L) using OpenFace [5, 6]. These metrics ensure that the rendered images accurately capture and reflect the target facial

Method	Sync-E(↓)/C(↑)	V-RMSE(↓)	A-RMSE(↓)	V-SA(↑)	A-SA(↑)	E-Acc(↑)
Ground truth	7.830/7.042	-	-	-	-	-
ER-NeRF [36]	10.109/4.225	0.479	0.502	0.500	0.500	27.3
GaussianTalker [12]	10.243/4.539	0.491	0.503	0.500	0.500	22.9
TalkingGaussian [37]	9.580/4.779	0.467	0.474	0.515	0.500	29.1
Ours	9.082/5.152	0.352	0.383	0.766	0.637	46.6

Table 3. We compare the models’ ability to reflect the desired emotion on the face. The best score is highlighted in **bold**.

action units. To evaluate the emotion consistency, we employ the valance and arousal root mean square error (V-RMSE and A-RMSE) [61], and valance and arousal sign agreement (V-SA and A-SA) [61]. Additionally, we utilize the top-3 emotion classification accuracy (E-Acc). We employ EmoNet [61] to extract valence, arousal, and emotion label from the rendered images.

4.2. Quantitative Results

We evaluate various metrics across three different scenarios, as reported in Tabs 1, 2, and 3. In *self-reconstruction* scenario, our method without the emotion branch achieves the best scores in pixel-based metrics, such as PSNR, SSIM, and LPIPS, as well as the landmark distance (LMD) and action unit error for the lower face (AUE-L) and upper face (AUE-U). Our method, which incorporates emotion and is trained on both emotional synthetic and original facial data, slightly compromises detail preservation, but it remains comparable to other baselines in pixel-based metrics, and outperforms them with higher lip synchronization confidence and lower action unit error for expressions. In *cross-domain audio* scenario, where we cannot use ground-truth images, we measure synchronization error (Sync-E) and confidence (Sync-C). Our method outperforms other methods in both Sync-E and Sync-C, demonstrating its ability to handle the cross-domain audio effectively. In *emotion-conditioned* scenario, we use Sync-E and Sync-C metrics to evaluate the lip-synchronization, and V-RMSE, A-RMSE, V-SA, and A-SA to evaluate the models’ ability to convey the desired emotion to the talking head. Other methods show V-SA and A-SA scores around 0.5, indicating that the valence and arousal values estimated from the rendered images are concentrated in only one quadrant of the valence-arousal circle. Additionally, they exhibit high V-RMSE and A-RMSE errors, along with low emotion classification accuracy. These suggest that these methods do not effectively reflect the desired emotions. In contrast, our model demonstrates superior performance across all metrics, confirming its ability to effectively convey the intended emotions on the face.

4.3. Qualitative Results

We present the qualitative results in Fig. 4. The word pronounced by the subject is highlighted in red. To manipulate facial emotion with our method, we use valence and arousal, shown below the pronounced word as V and A. To better understand which specific emotion the valence and arousal represent, the emotion label is displayed below the V and A values. For

Method	LPIPS (↓)	Sync-C(↑)	E-Acc (↑)
Ours w/o L_{normal}	0.0274	6.090	45.4
Ours w/o L_{sync}	0.0269	5.925	46.1
Combined face b.	0.0253	4.489	42.1
Ours w/o emo. b.	0.0255	6.270	25.3
Ours	0.0267	6.279	46.6

Table 4. Ablation study on loss functions and model architectures across different model configurations: ‘Ours w/o L_{normal} ’ (without normal map loss), ‘Ours w/o L_{sync} ’ (without sync loss), ‘Combined face b.’ (model combining face branch and emotion branch), ‘Ours w/o emo. b.’ (our model without the emotion branch), and ‘Ours’ (our full model). The best performance for each metric is highlighted in **bold**.

other methods, such as ER-NeRF [36], GaussianTalker [12] and TalkingGaussian [37], the action units are used to manipulate facial expressions. As shown in the blue dashed boxes in Fig. 4, action units have a limitation in expressing natural emotions. In contrast, our method expresses emotions around the eyes and mouth based on valence and arousal values. For lip synchronization, mismatches are highlighted with brown dashed boxes. Our method effectively synchronizes lip movements with speech audio while conveying the desired emotions.

4.4. Ablation Study

We conduct ablation study on loss functions and model architectures, as reported in Tab. 4. We use the self-reconstruction scenario to measure LPIPS and Sync-C, and the emotion-conditioned scenario to measure E-Acc. For *loss functions*, including the normal map loss L_{normal} and the sync loss L_{sync} , we compare the performance of our full model with ‘Ours w/o L_{normal} ’ and ‘Ours w/o L_{sync} ’. ‘Ours w/o L_{normal} ’ do not use L_{normal} and ‘Ours w/o L_{sync} ’ do not use L_{sync} , during training of EmoTalkingGaussian. L_{normal} impacts the quality of the rendered image, as evidenced by an increase in LPIPS. Similarly, L_{sync} influences lip sync accuracy, as reflected in changes in Sync-E/C. Additionally, for *model architectures*, we compare our full model with ‘Combined face b.’ and ‘Ours w/o Emo. b.’. ‘Combined face b.’ model renders emotional facial images using only the face manipulation network f^F in the face branch, where the network f^F takes valence, arousal, action units, and audio as inputs. ‘Ours w/o Emo. b.’ represents the our model without the emotion branch. ‘Combined face b.’ achieves the best LPIPS score but struggles with accurate lip synchronization. ‘Ours w/o Emo. b.’ fails to reflect emotion in the rendered image. While our full model shows slightly lower

performance in image quality, it outperforms other baseline in both lip synchronization and emotion control.

5. Conclusion

This paper introduces a novel 3D emotional talking head generation framework, EmoTalkingGaussian. Our framework can seamlessly utilize even new subject video containing highly sparse emotion representation without any need for additional data capturing. Benefiting from a lip-aligned emotional facial image generator, normal map loss, sync loss, and curated speech audio data, our method enables diverse emotion manipulation based on valence and arousal, synchronizing lip movements in the rendered image with the input audio while preserving high image quality.

Limitation. Depending on the emotion, the mouth in the synthesized image sometimes change dramatically, causing artifacts around the mouth region in the rendered image by EmoTalkingGaussian. This highlights a trade-off between image fidelity and the intensity of emotional expression.

Ethical consideration. There is potential for misuse, including in deepfake applications or deceptive media. To mitigate this, we strongly advocate for responsible use, ensuring that generated content is not used for misleading or harmful purposes. We aim to support efforts that aid in the detection and responsible development of deepfake technology.

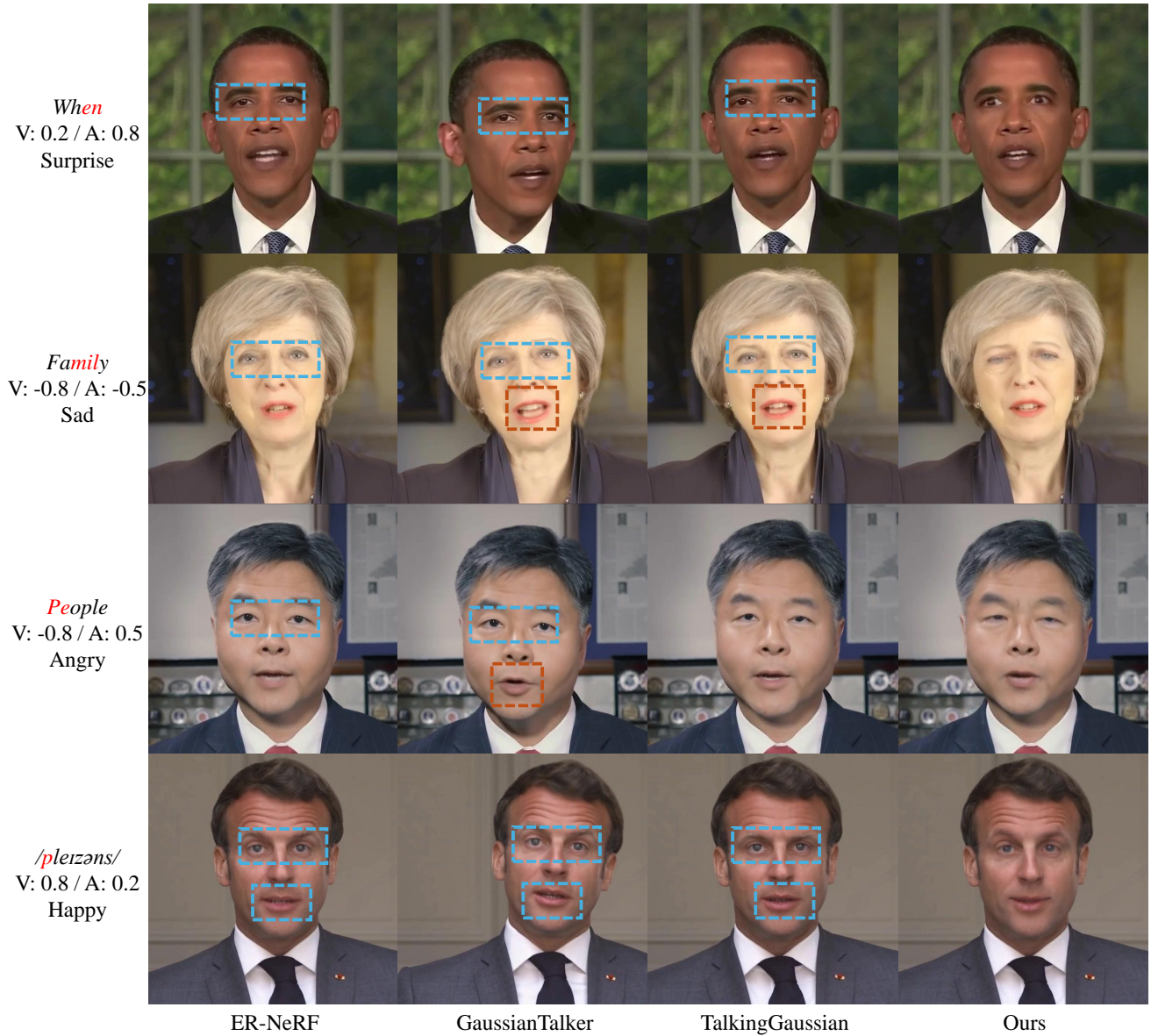


Figure 4. We present qualitative comparisons with other baselines, including ER-NeRF [36], GaussianTalker [12], and TalkingGaussian [37]. The word is displayed with the spoken word highlighted in red. The last sample shows the phonetic transcription. ‘V’ and ‘A’ stand for valence and arousal, and emotion labels indicate the emotion that ‘V’ and ‘A’ values represent. Emotional inconsistencies and lip mismatches are highlighted with blue and brown dashed boxes, respectively.

EmoTalkingGaussian: Continuous Emotion-conditioned Talking Head Synthesis

Supplementary Material

In this supplementary material, we provide implementation details; details of lip-aligned emotional face generator; rendering; details of training EmoTalkingGaussian; curated audio data; evaluation in emotion-conditioned scenario; attention visualization; inside-mouth normal map; limitations of simple fused approach; limitations of diffusion model; user study; and qualitative results. Additionally, for animatable results, please refer to the accompanying supplementary video, which includes the emotion-conditioned scenario comparison, valence-arousal interpolation, 360° valence-arousal interpolation (radius: 0.8), and dynamic emotion transitions during speech.

S1. Implementation Details

Our method is implemented using PyTorch. All experiments are conducted using RTX 4090 GPUs. We train the lip-aligned emotional face generator for 10 epochs using the Adam optimizer with a learning rate of 1×10^{-4} . The mouth branch, face branch, and emotion branch are each trained for 50,000 iterations, and the face canonical Gaussians are fine-tuned with an additional 20,000 iterations. We use the AdamW optimizer with a learning rate of 5×10^{-3} for the hash encoder and 5×10^{-4} for the other parts. The learning rates are adjusted using an exponential scheduler. The total training time is 2 hours. The loss weights are described in Secs. S2.2 and S4.3.

S2. Details of Lip-aligned Emotional Face Generator

S2.1. Pipeline

The overall framework of our lip-aligned emotional face generator g^{LEF} is illustrated in Fig. S1. EmoStyle [4] first creates a latent code \mathcal{W} from a source image I using an inversion module [4, 62]. It then produces an emotional latent code \mathcal{W}' by adding \mathcal{W} to an emotion modification vector d . The vector d is generated by EmoExtract M , which takes a concatenated vector ($f_{\text{emo}} \oplus \mathcal{W}$) as input. Here, f_{emo} represents the valence/arousal features derived from the valence/arousal input e through an up-sampling module. EmoStyle generates a facial image with lips that do not match those of the source image I .

To achieve lip alignment, a lip encoder E generates a lip embedding vector z_l from lip heatmaps H , which are extracted from the source image I using a LipDetector D_l [7]. A LipExtract module M_{lip} then produces a lip modification vector d_l by taking a concatenated vector ($z_l \oplus \mathcal{W}'$) as input. By adding d_l to the emotional latent code \mathcal{W}' , a lip-aligned emotional latent code \mathcal{W}'' is obtained. Finally, our generator employs StyleGAN2 [29] to generate a lip-aligned emotional facial image I^E from the latent code \mathcal{W}'' .

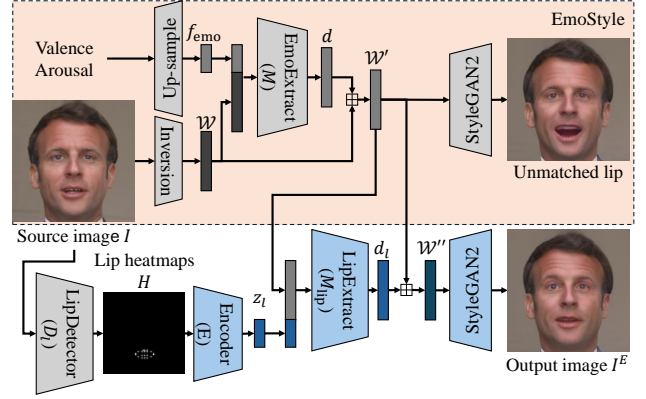


Figure S1. Overview of the lip-aligned emotional face generator. While EmoStyle [4] cannot produce lip-aligned emotional facial images, our generator creates such images by aligning lips based on lip heatmaps. \boxplus denotes vector summation.

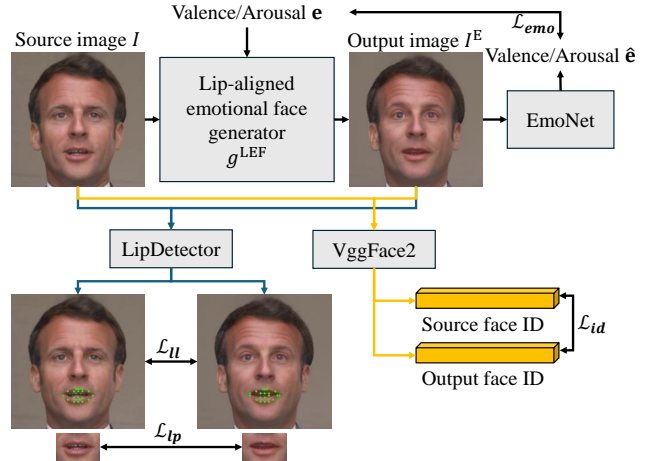


Figure S2. Lip landmark loss \mathcal{L}_l , lip pixel loss \mathcal{L}_{lp} , emotion loss \mathcal{L}_{emo} , identity loss \mathcal{L}_{id} are utilized to train the lip-aligned emotional face generator g^{LEF} . We use LipDetector [7], EmoNet [61], and VggFace2 [8].

S2.2. Losses

We train the encoder E and the LipExtract module M_{lip} , and fine-tune StyleGAN2 [29] using the following loss functions: lip landmark loss, lip pixel loss, regularization loss, emotion loss, and identity loss. These losses are illustrated in Fig. S2.

The lip landmark loss \mathcal{L}_l is defined as follows:

$$\mathcal{L}_l = \|\hat{L}_l - L_l\|_2^2, \quad (\text{S1})$$

where L_l and \hat{L}_l denote the lip landmarks extracted from the source image I and the output image I^E , respectively, using

the landmark detector [7]. This loss encourages the model to produce an output image I^E that closely aligns with the original lip structure of I , ensuring the positional accuracy of the generated lip region.

The lip pixel loss \mathcal{L}_{lp} is defined as follows:

$$\mathcal{L}_{lp} = \|\mathbb{M}_l \odot (I^E - I)\|_2^2, \quad (\text{S2})$$

where the lip region mask \mathbb{M}_l is applied to the pixel-wise difference between I^E and I . \mathbb{M}_l is a rectangular mask created based on the lip landmarks L_l , and \odot denotes element-wise multiplication. This loss penalizes differences in pixel values within the lip area, encouraging I^E to closely resemble I specifically in the lip region.

The regularization loss \mathcal{L}_{reg} is defined as follows:

$$\mathcal{L}_{reg} = \|d_l\|_2^2. \quad (\text{S3})$$

This loss prevents d_l from diverging.

The emotion loss \mathcal{L}_{emo} is defined as follows:

$$\mathcal{L}_{emo} = \|EmoNet(I^E) - e\|_2^2, \quad (\text{S4})$$

where *EmoNet* [61] outputs valence and arousal values \hat{e} from the output image I^E . This loss encourages the output image I^E to reflect the emotion specified by the input valence and arousal values e .

The identity loss \mathcal{L}_{id} is defined as follows:

$$\mathcal{L}_{id} = \|VF(I^E) - VF(I)\|_1 \quad (\text{S5})$$

where *VF* represents VggFace2 [8], which extracts identity embeddings corresponding to the face’s identity. This loss ensures that the identity of the output image I^E is preserved, matching that of the source image I .

Total training loss are expressed as follows:

$$\begin{aligned} \mathcal{L} = & \lambda_1 \cdot \mathcal{L}_{ll} + \lambda_2 \cdot \mathcal{L}_{lp} + \lambda_3 \cdot \mathcal{L}_{reg} \\ & + \lambda_4 \cdot \mathcal{L}_{emo} + \lambda_5 \cdot \mathcal{L}_{id}, \end{aligned} \quad (\text{S6})$$

where λ_1 , λ_2 , λ_3 , λ_4 , and λ_5 are 1, 5, 0.03, 0.2, and 1.5, respectively.

S3. Rendering

The i -th 3D Gaussian contains a position μ_i , a scaling factor s_i , a rotation quaternion q_i , an opacity value α_i , and a color c_i . The rendering process for 3D Gaussians is expressed as follows:

$$C(\mathbf{x}_p) = \sum_{i \in N} c_i \tilde{\alpha}_i \prod_{j=1}^{i-1} (1 - \tilde{\alpha}_j), \quad (\text{S7})$$

$$\mathcal{A}(\mathbf{x}_p) = \sum_{i \in N} \tilde{\alpha}_i \prod_{j=1}^{i-1} (1 - \tilde{\alpha}_j), \quad (\text{S8})$$

where $C(\mathbf{x}_p)$ and $\mathcal{A}(\mathbf{x}_p)$ represent color and opacity at pixel \mathbf{x}_p , respectively, as described in Eqs. 1 and 2 of the main

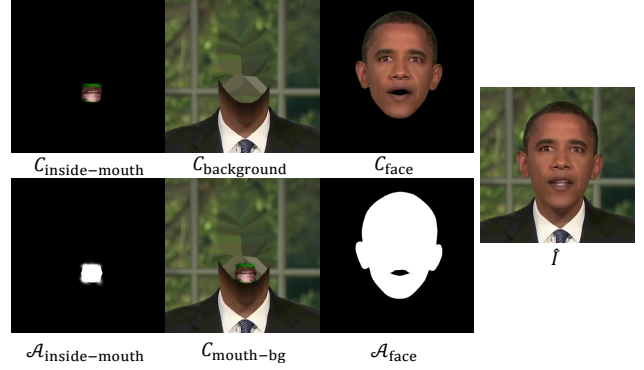


Figure S3. Examples of rendering are displayed, and their relationships are described in Eqs. S9 and S10.

paper. To generate a final image \hat{I} by combining the face color C_{face} , inside-mouth color $C_{inside-mouth}$, and background color $C_{background}$, we use the respective opacities \mathcal{A}_{face} and $\mathcal{A}_{inside-mouth}$ as follows:

$$\begin{aligned} C_{mouth-bg} = & C_{inside-mouth} \times \mathcal{A}_{inside-mouth} \\ & + C_{background} \times (1 - \mathcal{A}_{inside-mouth}), \end{aligned} \quad (\text{S9})$$

and

$$\hat{I} = C_{face} \times \mathcal{A}_{face} + C_{mouth-bg} \times (1 - \mathcal{A}_{face}), \quad (\text{S10})$$

where we blend the inside-mouth color $C_{inside-mouth}$ with the background color $C_{background}$ using the opacity $\mathcal{A}_{inside-mouth}$ to produce the combined inside-mouth and background color $C_{mouth-bg}$, and then blend this result with the face color C_{face} , using the opacity \mathcal{A}_{face} to produce the final image \hat{I} . The background color $C_{background}$ is provided, while $C_{inside-mouth}$ and $\mathcal{A}_{inside-mouth}$ are rendered from the inside-mouth deformed Gaussians θ^M , and C_{face} and \mathcal{A}_{face} are rendered from the emotionally deformed Gaussians θ^E . Examples of rendering are shown in Fig. S3.

S4. Details of Training EmoTalkingGaussian

S4.1. Improve Synthetic Emotional Facial Image

The initial generated image is produced by our lip-aligned emotional face generation network g^{LEF} , manipulates a source image by taking any valence/arousal e as input to generate an emotional face image that align with e . However, the generated images exhibit domain gaps compared to real images, particularly noticeable in artifacts such as blurry hair or irregularities in skin texture, as seen in the green boxes in column (a) and the yellow boxes in column (b) of Fig. S4. To reduce this gap, we use a cut-and-paste composite method. Rectangular regions around the eyes and mouth, which are expressive of emotion in the generated image, are cut and pasted onto the source image, as shown in column (c) of Fig. S4. These rectangular regions

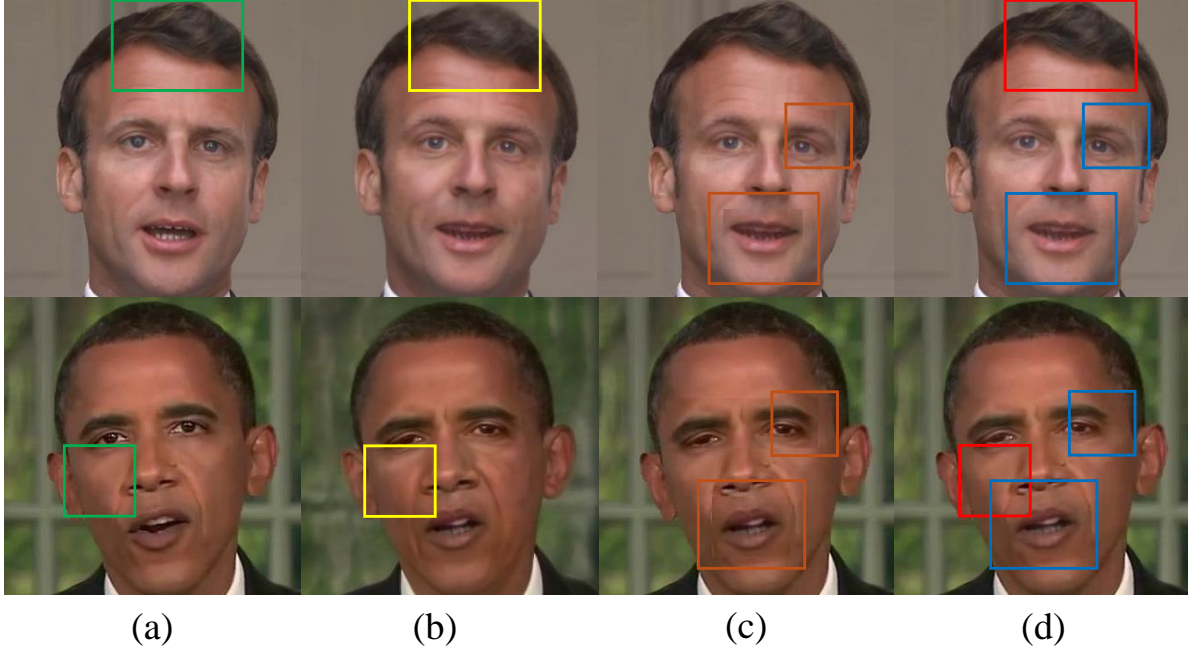


Figure S4. Columns (a), (b), (c), and (d) display source images, images generated by the lip-aligned emotional face generator g^{LEF} , simple cut-and-paste composite images, and seamless cloning results, respectively. The first row uses valence and arousal values of 0.6 and 0.2 (happy), while the second row applies values of -0.8 and 0.4 (angry). **Green** and **yellow** boxes indicate domain gaps, while **brown** boxes highlight boundary artifacts. **Red** and **blue** boxes demonstrate that seamless cloning effectively addresses both domain gaps and boundary artifacts, respectively.

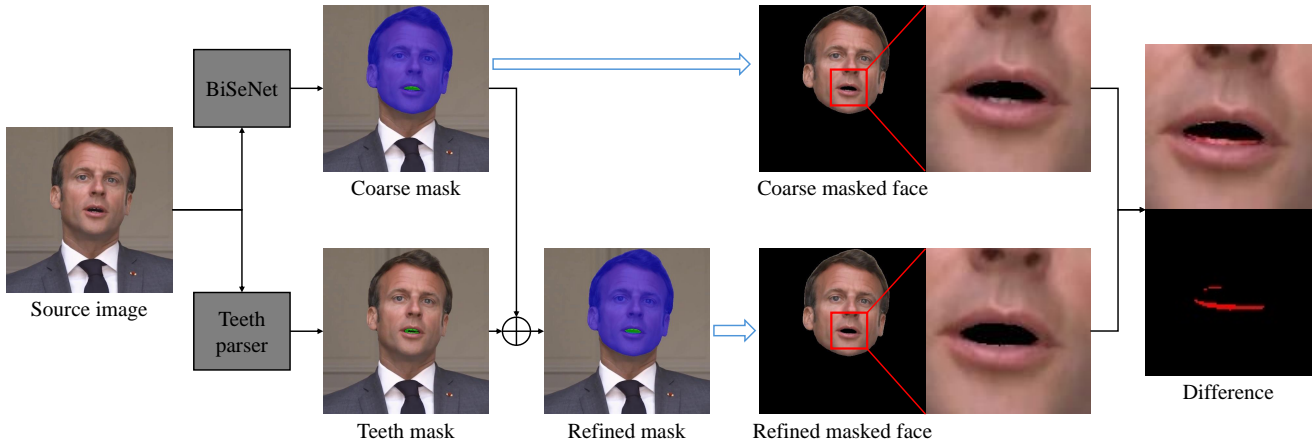


Figure S5. BiSeNet [68] estimates the coarse mask to parse the face and mouth regions, while the Teeth parser [37] estimates the teeth mask. These two masks are combined to create the refined mask, which more accurately separates the face and mouth compared to the coarse mask. The areas of discrepancy between the coarse and refined masks are highlighted in red, denoted as “Difference”, representing pixel differences between the face regions masked by each individual mask.

are determined using eye and mouth landmarks extracted from the generated image. However, while this approach reduces the domain gap by preserving realism in the source image and transferring emotion-expressive regions, it introduces boundary artifacts around the pasted areas, as shown in the brown boxes in column (c) of Fig. S4. To resolve this, we apply seamless cloning [49] that allows for smooth blending between the two

images. Unlike the simple cut-and-paste composite, which results in visible boundary artifacts, seamless cloning integrates textures and colors more naturally, effectively eliminating hard edges and creating a cohesive, realistic appearance, as seen in the red and blue boxes in column (d) of Fig S4. This realistic synthesis is leveraged for the training of our EmoTalkingGaussian.

S4.2. Processing Mask

Following TalkingGaussian [37], we utilize BiSeNet [68] and Teeth parser [37] to extract face and inside-mouth masks from a source image, as shown in Fig. S5. BiSeNet, pre-trained on CelebAMask-HQ dataset [34], generates a coarse mask which distinguishes face and mouth regions. By masking with the blue region of the coarse mask on the source image, as indicated by the above blue arrow, we extract the coarse masked face. However, as shown, this coarse mask cannot accurately separate the face and mouth regions, especially the teeth. Thus, to address this issue, the Teeth parser, trained on the EasyPortrait dataset [33], is employed to generate a teeth mask. By combining the coarse mask and the teeth mask, we create a refined mask. When the source image is masked using the blue region of the refined mask, as indicated by the below blue arrow, the teeth are no longer visible. The mask shown in red highlights the differences between the coarse masked face and the refined masked face. The green region of the refined mask is used to extract the inside-mouth region in Sec. S4.3.

S4.3. Ground Truth Preparation and Details of Training Losses

We prepare the ground truth data for each branch: the inside-mouth branch, face branch, and emotion branch, as shown in Fig. S6.

For the inside-mouth branch, we extract an inside-mouth region $I_{\text{mask}}(I_{\text{mask}}^M)$ from a source image I using a green region of the mask estimated in Sec. S4.2. The inside-mouth RGB image I_{mask}^M is used as I_{mask} in Eqs. 11 and 14 of the main paper. Accordingly, the inside-mouth canonical Gaussians θ_C^M are optimized using the following loss function:

$$\mathcal{L} = \mathcal{L}_1(\hat{I}_C^M, I_{\text{mask}}^M) + \gamma_1 \mathcal{L}_{\text{D-SSIM}}(\hat{I}_C^M, I_{\text{mask}}^M), \quad (\text{S11})$$

where \hat{I}_C^M denotes the RGB image rendered from θ_C^M , and γ_1 is 0.2. The inside-mouth region tri-plane hash encoder H^M and the inside-mouth region manipulate network f^M are trained using the following loss function:

$$\begin{aligned} \mathcal{L} = & \mathcal{L}_1(\hat{I}^M, I_{\text{mask}}^M) + \beta_1 \mathcal{L}_{\text{D-SSIM}}(\hat{I}^M, I_{\text{mask}}^M) \\ & + \beta_2 \mathcal{L}_{\text{LPIPS}}(\hat{I}^M, I_{\text{mask}}^M) + \beta_6 \mathcal{L}_{\text{sync}}, \end{aligned} \quad (\text{S12})$$

where \hat{I}^M denotes the RGB image rendered from inside-mouth deformed Gaussians θ^M , and β_1 , β_2 , and β_6 are 0.2, 0.2, and 0.05, respectively.

For the face branch, we extract a face region $I_{\text{mask}}(I_{\text{mask}}^F)$ from the source image I using the blue region of the estimated mask. Additionally, we create a masked face normal map N_{mask}^F using a normal estimator [3] along with the estimated mask. The face RGB image I_{mask}^F is used as I_{mask} in Eqs. 11 and 14 of the main paper, while the normal map N_{mask}^F is utilized in Eqs. 12 and 15 of the main paper. Accordingly, the face canonical

Gaussians θ_C^F are optimized using the following loss function:

$$\begin{aligned} \mathcal{L} = & \mathcal{L}_1(\hat{I}_C^F, I_{\text{mask}}^F) + \gamma_1 \mathcal{L}_{\text{D-SSIM}}(\hat{I}_C^F, I_{\text{mask}}^F) \\ & + \gamma_2 \mathcal{L}_1(\hat{N}_C^F, N_{\text{mask}}^F) + \gamma_3 \mathcal{L}_{\text{tv}}(\hat{N}_C^F) \\ & + \gamma_4 \|\Delta n\|, \end{aligned} \quad (\text{S13})$$

where \hat{I}_C^F and \hat{N}_C^F denote the RGB image and normal map rendered from θ_C^F , and γ_1 , γ_2 , γ_3 , and γ_4 are 0.2, 0.05, 0.005, and 0.001, respectively. The face region tri-plane hash encoder H^F and the face region manipulate network f^F are trained using the following loss function:

$$\begin{aligned} \mathcal{L} = & \mathcal{L}_1(\hat{I}^F, I_{\text{mask}}^F) + \beta_1 \mathcal{L}_{\text{D-SSIM}}(\hat{I}^F, I_{\text{mask}}^F) \\ & + \beta_2 \mathcal{L}_{\text{LPIPS}}(\hat{I}^F, I_{\text{mask}}^F) + \beta_3 \mathcal{L}_1(\hat{N}^F, N_{\text{mask}}^F) \\ & + \beta_4 \mathcal{L}_{\text{tv}}(\hat{N}^F) + \beta_5 \|\Delta n\| + \beta_6 \mathcal{L}_{\text{sync}}, \end{aligned} \quad (\text{S14})$$

where \hat{I}^F and \hat{N}^F denote the RGB image and normal map rendered from face deformed Gaussians θ^F , and β_1 , β_2 , β_3 , β_4 , β_5 , and β_6 are 0.2, 0.2, 0.05, 0.005, 0.001, and 0.05, respectively.

For the emotion branch, we generate the emotional facial image I^E using our lip-aligned emotional face generator g^{LEF} and seamless cloning algorithm described in Sec. S4.1. Similarly to the previous branches, we extract the RGB $I_{\text{mask}}(I_{\text{mask}}^E)$ and normal map N_{mask}^E for the face region using the estimated mask and the normal estimator [3]. The emotional face RGB image I_{mask}^E is used as I_{mask} in Eq. 17 of the main paper, while the emotional face normal map N_{mask}^E is utilized in Eq. 18 of the main paper. Accordingly, the emotion tri-plane hash encoder H^E and the emotion manipulation network f^E are trained using the following loss function:

$$\begin{aligned} \mathcal{L} = & \mathcal{L}_1(\hat{I}^E, I_{\text{mask}}^E) + \beta_1 \mathcal{L}_{\text{D-SSIM}}(\hat{I}^E, I_{\text{mask}}^E) \\ & + \beta_2 \mathcal{L}_{\text{LPIPS}}(\hat{I}^E, I_{\text{mask}}^E) + \beta_3 \mathcal{L}_1(\hat{N}^E, N_{\text{mask}}^E) \\ & + \beta_4 \mathcal{L}_{\text{tv}}(\hat{N}^E) + \beta_5 \|\Delta n\| + \beta_6 \mathcal{L}_{\text{sync}}, \end{aligned} \quad (\text{S15})$$

where \hat{I}^E and \hat{N}^E denote the RGB image and normal map rendered from emotionally deformed Gaussians θ^E , and β_1 , β_2 , β_3 , β_4 , β_5 , and β_6 are 0.2, 0.2, 0.05, 0.005, 0.001, and 0.001, respectively.

After finishing training, the face canonical Gaussians θ_C^F are further optimized to erase artifacts around face border using the following loss function, focusing only on optimizing the Gaussian's opacity α and color c :

$$\begin{aligned} \mathcal{L} = & \mathcal{L}_1(\hat{I}, I) + \eta_1 \mathcal{L}_{\text{D-SSIM}}(\hat{I}, I) \\ & + \eta_2 \mathcal{L}_{\text{LPIPS}}(\hat{I}, I), \end{aligned} \quad (\text{S16})$$

where \hat{I} represents the image rendered by Eq. S10, η_1 and η_2 are 0.2 and 0.5, respectively.

S5. Curated Audio Data

We synthesize curated audio data to improve lip synchronization by using ChatGPT [43] and text-to-speech network [18]. The 10 text descriptions of the audio are listed as follows:

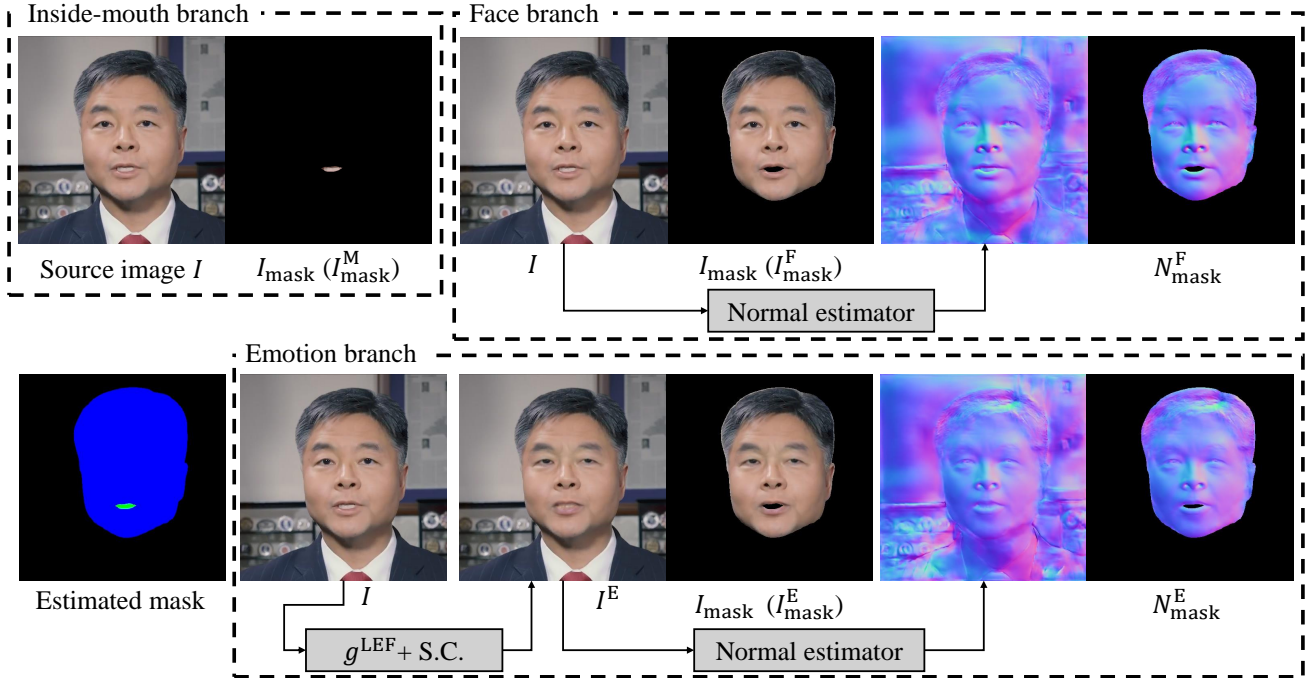


Figure S6. Preparation of ground truth data for training EmoTalkingGaussian involves the lip-aligned emotional face generator g^{LEF} combined with seamless cloning (described in Sec. S4.1 and ‘S.C.’ stands for seamless cloning), the normal estimator [3], and the estimated mask (described in Sec. S4.2).

Sentence 1. The quick brown fox jumps over the lazy dog.

- **Phonetic Notation:** /ðɪ:/, /kwɪk/, /braʊn/, /fɔːks/, /dʒʌmpz/, /'oʊvə/, /ðɪ:/, /'leɪzi/, /dɔːg/.
- **Sound Coverage:** Includes nearly all English consonants and vowels.
- **Liaison:** /t/ liaison occurs in “over the” (/oʊvə ðə/).
- **Stress:** Content words such as “quick”, “brown”, “fox”, “jumps”, “over”, “lazy”, and “dog” are stressed.
- **Weak Form:** “The” (/ðə/).

Sentence 2. She’s going to buy some new clothes at the mall.

- **Phonetic Notation:** /ʃiːz/, /'ɡoʊɪŋ/, /tuː/, /baɪ/, /sʌm/, /nuː/, /kloʊðz/, /æt/, /ðɪ:/, /mɑːl/.
- **Diphthongs:** /aɪ/ (buy), /oʊ/ (clothes).
- **Weak Forms:**
 - “to”: /tə/.
 - “some”: /səm/.
 - “at”: /ət/.
 - “the”: /ðə/.

Sentence 3. I can’t believe it’s already half past eight!

- **Phonetic Notation:** /aɪ/, /kænt/, /bɪ'liːv/, /ɪts/, /ɑːl'reɪdi/, /hæf/, /pæst/, /eɪt/.
- **Contractions:** “can’t” as /kænt/, “it’s” as /ɪts/.
- **Stress:** “can’t”, “believe”, “already”, “half”, and “eight” are stressed.

- **Silent Letters:** The “l” in “half” is silent.

Sentence 4. Do you want to grab some water?

- **Phonetic Notation:** /duː/, /juː/, /wɑːnt/, /tuː/, /græb/, /sʌm/, /wɑːtə/.
- **R-pronunciation:** “water” is pronounced as /wɑːtə/.
- **Weak Forms:**
 - “to”: /tə/.
 - “some”: /səm/.

Sentence 5. Better late than never, they say.

- **Phonetic Notation:** /betə/, /leɪt/, /ðə æn/, /'nevə/, /ðeɪ/, /seɪ/
- **Flapping:** “better” sounds like /betə/ with a flapped t.
- **Liaison:** Connection in “than never” with n.
- **Weak Form:** “than” (ðən).

Sentence 6. She needs to see the doctor immediately.

- **Phonetic Notation:** /ʃiː/, /niːds/, /tuː/, /siː/, /ðɪː/, /'dɑːktə/, /ɪ'miːdiətli/
- **Long Vowel:** Long /iː/ sounds in “needs” and “see”.
- **Stress:** “needs”, “see”, “doctor”, and “immediately” are stressed.
- **Weak Forms:**
 - “to”: /tə/.
 - “the”: /ðə/.

Sentence 7. Did you eat yet?

- **Phonetic Notation:** /dɪd/, /ju:/, /ɪt/, /jet/
- **Liaison /j/:** “Did you” sounds like /dɪdʒu:/.
- **Stress:** “eat” is stressed.

Sentence 8. Next stop is Central Park.

- **Phonetic Notation:** /nekst/, /stɑ:p/, /ɪz/, /'sentrəl/, /pɑ:rk/
- **Consonant Cluster:** /'sentrəl/ in “central”.
- **Elision:** The “t” is dropped in “next stop”, sounding like /nekst stɑ:p/.
- **Stress:** “next”, “stop”, “Central”, and “Park” are stressed.

Sentence 9. An unknown number called me yesterday.

- **Phonetic Notation:** /æn/, /ʌn'nəʊn/, /'nʌmbə/, /kɑ:ld/, /mi:/, /'jestədeɪ/
- **Double Consonant:** The n is lengthened in “unknown” (/n'n/).
- **R-pronunciation:** The word “number” has an r-colored schwa vowel (əɾ).
- **Stress:** “unknown”, “number”, “called”, and “yesterday” are stressed.
- **Weak Form:** “An” (ən).

Sentence 10. We can meet at the café if you'd like.

- **Phonetic Notation:** /wi:/, /k æn/, /mi:t/, /æt/, /ðɪ:/, /kæf eɪ/, /ɪf/, /ju:d/, /laɪk/
- **Contraction:** “you'd” pronounced as /ju:d/.
- **Stress:** “meet”, “café”, and “like” are stressed.
- **Weak Forms:**
 - “can”: /kən/.
 - “at”: /ət/.
 - “the”: /ðə/.

S6. Evaluation in Emotion-conditioned Scenario

We evaluate our method against state-of-the-art approaches across various scenarios. While prior studies [12, 36, 37] primarily focused on self-reconstruction and cross-domain audio scenarios, this paper introduces the emotion-conditioned scenario for the first time. This new scenario allows us to evaluate each method’s ability to accurately reflect the desired emotion in the rendered face. To evaluate them, we first select 12 valence and arousal values:

[0.74,0.31],[0.31,0.74],[−0.31,0.74],[−0.74,0.31], [−0.74,−0.31],[−0.31,−0.74],[0.31,−0.74], [0.74,−0.31],[0.35,0.35],[−0.35,0.35], [−0.35,−0.35],[0.35,−0.35]. Specifically, the valence-arousal points with a radius of 0.8 are selected by dividing 360° into 8, with each point separated by a 45° interval. Similarly, the valence-arousal points with a radius of 0.5 are chosen by dividing 360° into 4, placing each point at a 90° interval. This

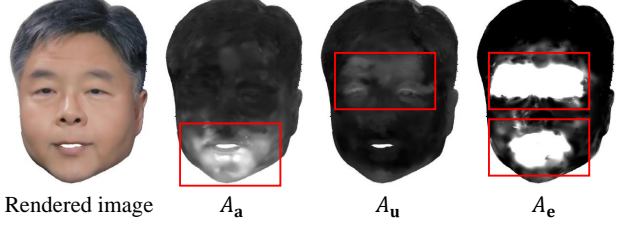


Figure S7. Attention visualization. A_a , A_u , and A_e represent attention maps for audio, action units, and valence/arousal, respectively.

approach ensures that the valence-arousal points are evenly distributed around the circle.

Using these valence-arousal points, our model conveys emotion directly. In contrast, other methods [12, 36, 37] cannot utilize valence-arousal values directly. Instead, they rely on EmoStyle [4] to generate each individual’s emotional face based on valence-arousal points. Action units are then extracted from this generated image using OpenFace [6], which are subsequently used to adjust facial expressions when rendering the talking heads in these methods [12, 36, 37].

We measure V-RMSE, A-RMSE, V-SA, and A-SA. The root mean square error RMSE is defined as:

$$\text{RMSE} = \sqrt{\frac{1}{N} \sum_{i=1}^N (\mathcal{E}_i^{\text{pred}} - \mathcal{E}_i^{\text{true}})^2}, \quad (\text{S17})$$

where $\mathcal{E}_i^{\text{true}}$ denotes the selected valence or arousal point used as the condition, $\mathcal{E}_i^{\text{pred}}$ represents the valence or arousal value estimated by EmoNet [61] for the i -th frame sample, and N denotes the number of frames.

The sign agreement SA is defined as:

$$\text{SA} = \frac{1}{N} \sum_{i=1}^N \mathbb{I}(\text{sign}(\mathcal{E}_i^{\text{pred}}) == \text{sign}(\mathcal{E}_i^{\text{true}})), \quad (\text{S18})$$

where $\mathbb{I}(\cdot)$ is the indicator function that returns 1 if the condition inside is true and 0 if false. The $\text{sign}(\cdot)$ function outputs 1 if the input is positive, -1 if it is negative, and 0 if it is zero.

Additionally, we utilize frame-wise emotion classification accuracy. Since assigning a single precise emotion class label to each valence-arousal pair is challenging, we evaluate the performance using top-3 accuracy. EmoNet [61] predicts emotion class labels from images rendered by each talking head synthesis model, and the accuracy is measured by comparing the predicted class labels with the predefined emotion class labels. Predefined emotion class labels are assigned to each valence-arousal point as follows:

[0.74,0.31]: Happy, [0.31,0.74]: Surprise,
 [−0.31,0.74]: Angry, [−0.74,0.31]: Disgust,
 [−0.74,−0.31]: Sad, [−0.31,−0.74]: Sad,
 [0.31,−0.74]: Contempt, [0.74,−0.31]: Contempt,

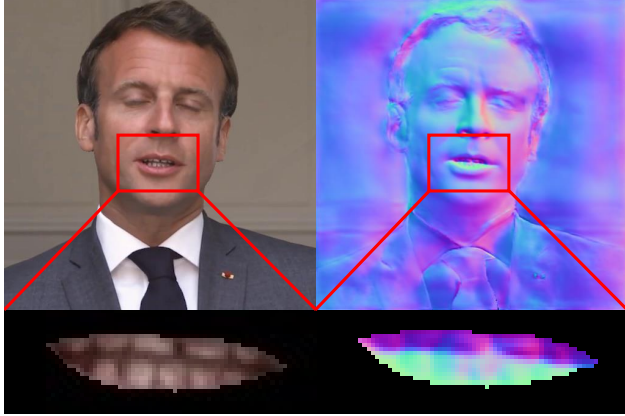


Figure S8. The normal map is estimated by the method in [3]. The row below shows zoomed-in RGB and normal map images of the inside-mouth region, masked with the refined mask described in Sec. S4.2.

$[0.35, 0.35]$: Happy, $[-0.35, 0.35]$: Angry,
 $[-0.35, -0.35]$: Sad, $[0.35, -0.35]$: Contempt.

S7. Attention Visualization

We apply an attention mechanism before feeding the audio features \mathbf{a} and action units \mathbf{u} into the manipulation network f^F , as described in Eq. 5 of the main paper, and the valence/arousal \mathbf{e} into the emotion manipulation network f^E , as described in Eq. 6 of the main paper. The attention maps, denoted as $A_{\mathbf{a}}$, $A_{\mathbf{u}}$, and $A_{\mathbf{e}}$, are visualized in Fig. S7. The audio attention map $A_{\mathbf{a}}$ focuses primarily on the regions around the lips and jaw, capturing movements conditioned on input speech audio. The action units attention map $A_{\mathbf{u}}$ emphasizes areas around the eyelids and eyebrows, highlighting expressive changes based on action units, such as eye blinking and eyebrow movements. Meanwhile, the emotion attention map $A_{\mathbf{e}}$ concentrates on the mouth and eyes, emphasizing features crucial for reflecting emotional expressions.

S8. Inside-mouth Normal Map

Fig. S8 presents an RGB image and a normal map of the inside-mouth region. The normal map is estimated by [3]. The normal map of the inside-mouth region is not well estimated, as shown by the inconsistency between the upper and lower teeth. It leads to unstable optimization of the 3D canonical Gaussians θ_C^M , along with unstable training of the tri-plane hash encoder H^M and the manipulation network f^M for inside-mouth region.

S9. Limitations of Simple Fused Approach

We fuse TalkingGaussian [37] with our lip-aligned emotional face generator g^{LEF} and visualize the results in Fig. S9. Although our face generator g^{LEF} adjusts emotions based on a valence/arousal setting of $(0.5, 0.1)$, which corresponds to a



Figure S9. The results of directly applying our lip-aligned emotional face generator g^{LEF} to the results of TalkingGaussian (TG) [37].

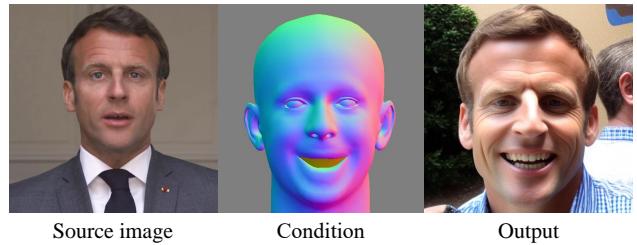


Figure S10. Result from diffusion-based models, Arc2Face [45], and ControlNet [71].

slight smile, it does not align the teeth shape with the output of TalkingGaussian.

S10. Limitations of Diffusion-based Model

There are two primary approaches to generate emotional facial images: GAN-based models and diffusion-based models. In our task, there are numerous possible combinations of valence, arousal, and video frames, making it impractical to generate and store emotional facial images in advance. Therefore, we generate the images during the training of EmoTalkingGaussian. However, diffusion-based face generation models are inherently slow, which inevitably increases training time. Additionally, these models tend to significantly alter the pose and style of the source face image, often resulting in a lack of synchronization with the source image and producing unrealistic appearances. To modify the emotion in facial images using diffusion-based models, we use Arc2Face [45] and ControlNet [71], which require conditions rendered from the FLAME model [38]. We utilize the normal map rendered from the FLAME mesh as the condition. The FLAME mesh incorporates pose and shape parameters obtained from the source image, along with expression parameters that represent smiling-related features. Although these methods enable changes in emotion, as shown in Fig. S10, the resulting face undergoes significant alterations and appears unnatural. Therefore, we utilize GAN-based models for more efficient and effective generation of emotional facial images.

S11. User Study

In Table S1, we report the results of a user study conducted to evaluate the reflection of emotions, lip synchronization to the audio, and overall quality. While lip synchronization performance is comparable across models, our method demonstrates the highest capability in reflecting the desired emotions and receives the most selections for overall quality.

	SD1 (%)	SD2 (%)	SD3 (%)
ER-NeRF [36]	4.17	15.83	16.25
GaussianTalker [12]	10.00	31.67	25.84
TalkingGaussian [37]	5.42	14.58	11.25
Ours	69.58	32.92	43.33
none	10.83	5.00	3.33

Table S1. The proportion of videos selected by users for each evaluation criterion is presented in this table. ‘SD1’ denotes Standard 1, representing the proportion of videos chosen by users as best reflecting emotions. ‘SD2’ represents Standard 2, indicating the proportion of videos selected as best in lip synchronization to the audio, and ‘SD3’ denotes Standard 3, reflecting the proportion of videos rated as best in overall quality.

S12. Qualitative Results

We present the qualitative results across three scenarios: self-reconstruction, cross-domain audio, and emotion-conditioned generation, as shown in Figs. S11, S12, and S13. For the each scenario, we compare our results with those of other models, including ER-NeRF [36], GaussianTalker [12], and TalkingGaussian [37]. In the emotion-conditioned scenario, we demonstrate the results using valence and arousal values of 0.31 and 0.74, respectively. Additionally, we illustrate our method’s ability to reflect the desired emotion in the rendered face, as shown in Fig S14. Furthermore, we showcase the transition of emotions by changing the valence and arousal values. For a detailed view of the continuous transitions in facial emotions and additional results, please refer to the supplementary video, including emotion-conditioned scenario comparison, valence-arousal interpolation, 360° valence-arousal interpolation (radius: 0.8), and dynamic emotion transitions during speech.

References

- [1] <https://www.pexels.com/>. 1
- [2] Rameen Abdal, Peihao Zhu, Niloy J Mitra, and Peter Wonka. Styleflow: Attribute-conditioned exploration of stylegan-generated images using conditional continuous normalizing flows. *ACM Transactions on Graphics (ToG)*, 2021. 3
- [3] Victoria Fernandez Abrevaya, Adnane Boukhayma, Philip H.S. Torr, and Edmond Boyer. Cross-modal deep face normals with deactivable skip connections. In *CVPR*, 2020. 2, 5, 4, 7
- [4] Bitu Azari and Angelica Lim. Emostyle: One-shot facial expression editing using continuous emotion parameters. In *WACV*, 2024. 2, 3, 4, 5, 6, 1
- [5] Tadas Baltrušaitis, Marwa Mahmoud, and Peter Robinson. Cross-dataset learning and person-specific normalisation for automatic action unit detection. In *IEEE international conference and workshops on automatic face and gesture recognition (FG)*, 2015. 6
- [6] Tadas Baltrušaitis, Amir Zadeh, Yao Chong Lim, and Louis-Philippe Morency. Openface 2.0: Facial behavior analysis toolkit. In *IEEE International Conference on Automatic Face and Gesture Recognition (FG 2018)*, 2018. 4, 6
- [7] Adrian Bulat and Georgios Tzimiropoulos. How far are we from solving the 2d & 3d face alignment problem?(and a dataset of 230,000 3d facial landmarks). In *ICCV*, 2017. 5, 1, 2
- [8] Qiong Cao, Li Shen, Weidi Xie, Omkar M Parkhi, and Andrew Zisserman. Vggface2: A dataset for recognising faces across pose and age. In *IEEE international conference on automatic face & gesture recognition (FG 2018)*, 2018. 1, 2
- [9] Aggelina Chatziagapi, ShahRukh Athar, Abhinav Jain, MV Rohith, Vimal Bhat, and Dimitris Samaras. Lipnerf: What is the right feature space to lip-sync a nerf? In *IEEE International Conference on Automatic Face and Gesture Recognition*, 2023. 2
- [10] Lele Chen, Zhiheng Li, Ross K Maddox, Zhiyao Duan, and Chenliang Xu. Lip movements generation at a glance. In *ECCV*, 2018. 3, 6
- [11] Lele Chen, Ross K Maddox, Zhiyao Duan, and Chenliang Xu. Hierarchical cross-modal talking face generation with dynamic pixel-wise loss. In *CVPR*, 2019. 3
- [12] Kyusun Cho, JoungBin Lee, Heeji Yoon, Yeobin Hong, Jaehoon Ko, Sangjun Ahn, and Seungryong Kim. Gaussiantalker: Real-time talking head synthesis with 3d gaussian splatting. In *ACM Multimedia 2024*, 2024. 2, 3, 6, 7, 9, 8, 10, 11
- [13] Yunjey Choi, Minje Choi, Munyoung Kim, Jung-Woo Ha, Sunghun Kim, and Jaegul Choo. Stargan: Unified generative adversarial networks for multi-domain image-to-image translation. In *CVPR*, 2018. 2, 3
- [14] Joon Son Chung and Andrew Zisserman. Out of time: automated lip sync in the wild. In *ACCV Workshop*, 2017. 2, 3, 5, 6
- [15] Stefano d’Apolito, Danda Pani Paudel, Zhiwu Huang, Andres Romero, and Luc Van Gool. Ganmut: Learning interpretable conditional space for gamut of emotions. In *CVPR*, 2021. 2
- [16] Hui Ding, Kumar Sricharan, and Rama Chellappa. Exprgan: Facial expression editing with controllable expression intensity. In *AAAI*, 2018. 2
- [17] Zheng Ding, Xuaner Zhang, Zhihao Xia, Lars Jebe, Zhuowen Tu, and Xiuming Zhang. Diffusionrig: Learning personalized priors for facial appearance editing. In *CVPR*, 2023. 3
- [18] Pierre Nicolas Durette. gtts: Python library and cli tool to interface with google translate’s text-to-speech api, 2024. 2, 4, 5
- [19] Paul Ekman and Wallace V Friesen. Facial action coding system. *Environmental Psychology & Nonverbal Behavior*, 1978. 1, 2
- [20] Yuan Gan, Zongxin Yang, Xihang Yue, Lingyun Sun, and Yi Yang. Efficient emotional adaptation for audio-driven talking-head generation. In *ICCV*, 2023. 3, 6
- [21] Yudong Guo, Keyu Chen, Sen Liang, Yong-Jin Liu, Hujun Bao, and Juyong Zhang. Ad-nerf: Audio driven neural radiance fields for talking head synthesis. In *ICCV*, 2021. 2, 3, 6
- [22] A Hannun. Deep speech: Scaling up end-to-end speech recognition. *arXiv:1412.5567*, 2014. 4



Figure S11. We present the qualitative comparisons in the self-reconstruction scenario against other methods, including ER-NeRF [36], GaussianTalker [12], and TalkingGaussian [37]. Misalignment with the ground truth is highlighted using gray arrows for discrepancies in the eyebrows and forehead wrinkles, blue arrows for blinking errors, and red boxes for lip misalignment.

- [23] Erik Härkönen, Aaron Hertzmann, Jaakko Lehtinen, and Sylvain Paris. Ganspace: Discovering interpretable gan controls. *NIPS*, 2020. 3
- [24] Qianyun He, Xinya Ji, Yicheng Gong, Yuanxun Lu, Zhengyu Diao, Linjia Huang, Yao Yao, Siyu Zhu, Zhan Ma, Songcen Xu, et al. Emotalk3d: High-fidelity free-view synthesis of emotional 3d talking head. In *ECCV*, 2024. 2, 3
- [25] Jonathan Ho, Ajay Jain, and Pieter Abbeel. Denoising diffusion probabilistic models. *NIPS*, 2020. 3
- [26] Shoukang Hu, Tao Hu, and Ziwei Liu. Gauhuman: Articulated gaussian splatting from monocular human videos. In *CVPR*, 2024. 2
- [27] Yuheng Jiang, Zehao Shen, Penghao Wang, Zhuo Su, Yu Hong, Yingliang Zhang, Jingyi Yu, and Lan Xu. Hifi4g: High-fidelity human performance rendering via compact gaussian splatting. In *CVPR*, 2024. 2
- [28] Yingwenqi Jiang, Jiadong Tu, Yuan Liu, Xifeng Gao, Xiaoxiao Long, Wenping Wang, and Yuexin Ma. Gaussianshader: 3d gaussian splatting with shading functions for reflective surfaces. In *CVPR*, 2024. 4
- [29] Tero Karras, Samuli Laine, Miika Aittala, Janne Hellsten, Jaakko Lehtinen, and Timo Aila. Analyzing and improving the image quality of stylegan. In *CVPR*, 2020. 3, 5, 1
- [30] Bernhard Kerbl, Georgios Kopanas, Thomas Leimkühler, and George Drettakis. 3d gaussian splatting for real-time radiance field rendering. *ACM Trans. Graph.*, 2023. 2, 3, 4
- [31] Siavash Khodadadeh, Shabnam Ghadar, Saied Motiian, Wei-An Lin, Ladislau Bölöni, and Ratheesh Kalarot. Latent to latent: A learned mapper for identity preserving editing of multiple face attributes in stylegan-generated images. In *WACV*, 2022. 3
- [32] Dimitrios Kollias and Stefanos Zafeiriou. Va-stargan: Continuous affect generation. In *Advanced Concepts for Intelligent Vision Systems: 20th International Conference, ACIVS 2020, Auckland, New Zealand, February 10–14, 2020, Proceedings 20*, 2020. 2, 3



Figure S12. We present qualitative comparisons in the cross-domain audio scenario against other methods, including ER-NeRF [36], GaussianTalker [12], and TalkingGaussian [37]. Lip misalignment with the ground truth is highlighted using red boxes.

- [33] Karina Kvanchiani, Elizaveta Petrova, Karen Efremyan, Alexander Sautin, and Alexander Kapitanov. Easyportrait–face parsing and portrait segmentation dataset. *arXiv:2304.13509*, 2023. 4
- [34] Cheng-Han Lee, Ziwei Liu, Lingyun Wu, and Ping Luo. Maskgan: Towards diverse and interactive facial image manipulation. In *CVPR*, 2020. 4
- [35] Dongze Li, Kang Zhao, Wei Wang, Yifeng Ma, Bo Peng, Yingya Zhang, and Jing Dong. S³d-nerf: Single-shot speech-driven neural radiance field for high fidelity talking head synthesis. In *ECCV*, 2024. 3
- [36] Jiahe Li, Jiawei Zhang, Xiao Bai, Jun Zhou, and Lin Gu. Efficient region-aware neural radiance fields for high-fidelity talking portrait synthesis. In *ICCV*, 2023. 2, 3, 4, 6, 7, 9, 8, 10, 11
- [37] Jiahe Li, Jiawei Zhang, Xiao Bai, Jin Zheng, Xin Ning, Jun Zhou, and Lin Gu. Talkinggaussian: Structure-persistent 3d talking head synthesis via gaussian splatting. In *ECCV*, 2024. 1, 2, 3, 4, 5, 6, 7, 9, 8, 10, 11
- [38] Tianye Li, Timo Bolkart, Michael J Black, Hao Li, and Javier Romero. Learning a model of facial shape and expression from 4d scans. *ACM Trans. Graph.*, 2017. 3, 7
- [39] Alexandra Lindt, Pablo Barros, Henrique Siqueira, and Stefan Wermter. Facial expression editing with continuous emotion labels. In *IEEE International Conference on Automatic Face and Gesture Recognition*, 2019. 2
- [40] Ben Mildenhall, Pratul P Srinivasan, Matthew Tancik, Jonathan T Barron, Ravi Ramamoorthi, and Ren Ng. Nerf: Representing scenes as neural radiance fields for view synthesis. *Communications of the ACM*, 2021. 2, 3
- [41] Mehdi Mirza. Conditional generative adversarial nets. *arXiv:1411.1784*, 2014. 2
- [42] Gyeongseok Moon, Takaaki Shiratori, and Shunsuke Saito. Expressive whole-body 3D gaussian avatar. In *ECCV*, 2024. 2
- [43] OpenAI. Chatgpt, 2024. 5, 4
- [44] Haokai Pang, Heming Zhu, Adam Kortylewski, Christian

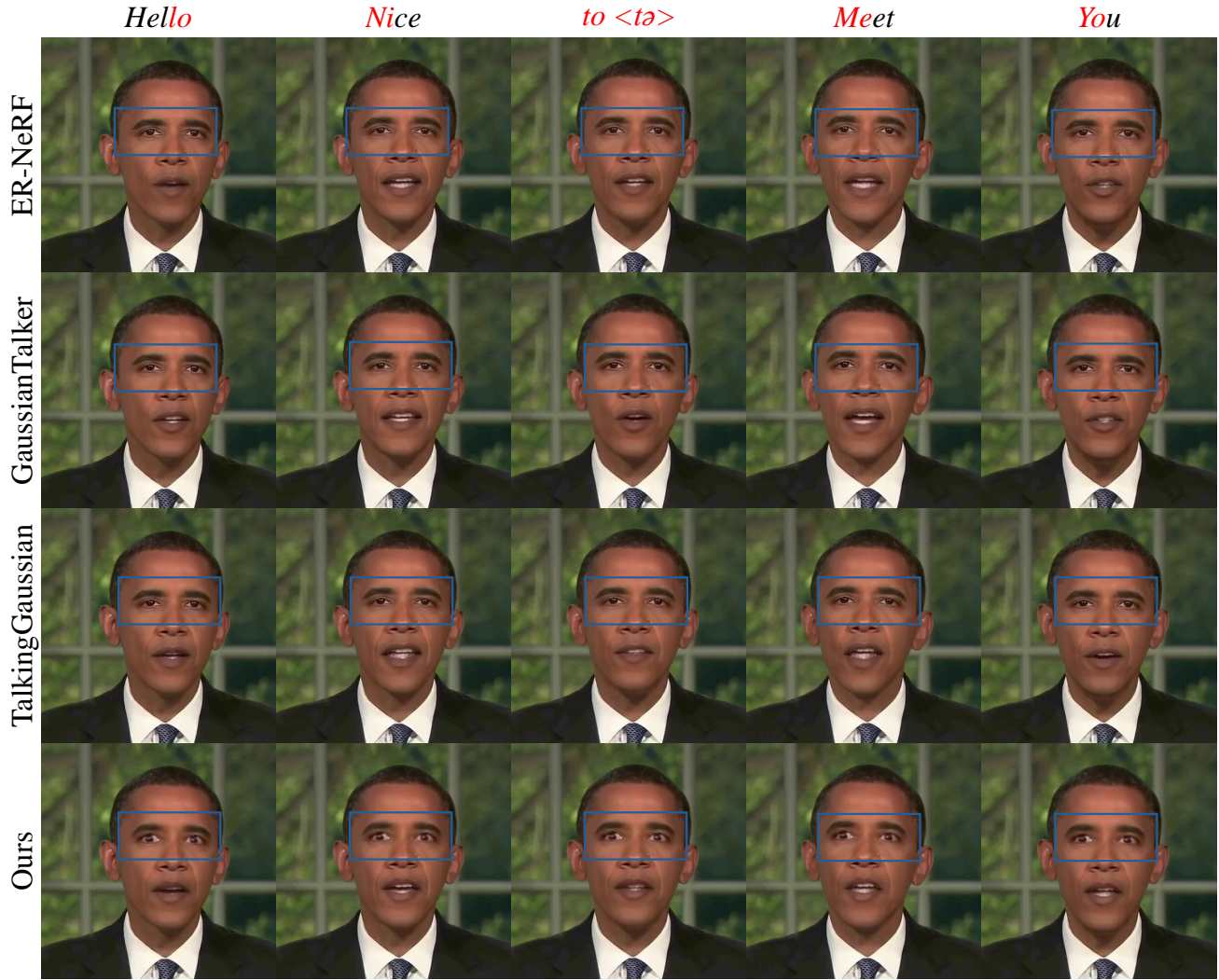


Figure S13. We demonstrate qualitative comparisons in the emotion-conditioned scenario against other methods, including ER-NeRF [36], GaussianTalker [12], and TalkingGaussian [37]. The valence and arousal values are set to 0.31 and 0.74, respectively, to represent the emotion of surprise. We use blue boxes to highlight the area around the eyes, emphasizing the expression of emotion. The words being pronounced by the speaker in each column are highlighted in red.

- Theobalt, and Marc Habermann. Ash: Animatable gaussian splats for efficient and photoreal human rendering. In *CVPR*, 2024. 2
- [45] Foivos Paraperas Papantoniou, Alexandros Lattas, Stylianos Moschoglou, Jiankang Deng, Bernhard Kainz, and Stefanos Zafeiriou. Arc2face: A foundation model for id-consistent human faces. In *ECCV*, 2024. 3, 7
- [46] Reni Paskaleva, Mykyta Holubakha, Andela Ilic, Saman Motamed, Luc Van Gool, and Danda Paudel. A unified and interpretable emotion representation and expression generation. In *CVPR*, 2024. 3
- [47] Or Patashnik, Zongze Wu, Eli Shechtman, Daniel Cohen-Or, and Dani Lischinski. Styleclip: Text-driven manipulation of stylegan imagery. In *ICCV*, 2021. 3
- [48] Ziqiao Peng, Wentao Hu, Yue Shi, Xiangyu Zhu, Xiaomei Zhang, Hao Zhao, Jun He, Hongyan Liu, and Zhaoxin Fan. Synctalk: The devil is in the synchronization for talking head synthesis. In *CVPR*, 2024. 2
- [49] Patrick Pérez, Michel Gangnet, and Andrew Blake. Poisson image editing. In *Seminal Graphics Papers: Pushing the Boundaries, Volume 2*. 2023. 3
- [50] Chandradeep Pokhariya, Ishaan Nikhil Shah, Angela Xing, Zekun Li, Kefan Chen, Avinash Sharma, and Srinath Sridhar. Manus: Markerless grasp capture using articulated 3d gaussians. In *CVPR*, 2024. 2
- [51] KR Prajwal, Rudrabha Mukhopadhyay, Vinay P Nambodiri, and CV Jawahar. A lip sync expert is all you need for speech to lip generation in the wild. In *Proceedings of the 28th ACM international conference on multimedia*, 2020. 3
- [52] Albert Pumarola, Antonio Agudo, Aleix M Martinez, Alberto Sanfeliu, and Francesc Moreno-Noguer. Ganimation:



Figure S14. We demonstrate our proposed method’s ability to reflect the desire emotion in the rendered face. Each row utilizes specific valence-arousal values: (0.3, 0.7), (0.8, -0.5), (-0.6, 0.5), and (-0.8, -0.2). The first row changes the valence/arousal from (0.3, 0.7) to (-0.8, 0.5). The second row changes the valence/arousal from (0.8, -0.5) to (0.6, 0.5). The third row changes the valence/arousal from (-0.6, 0.4) to (0.8, 0.2). The fourth row changes the valence/arousal from (-0.8, -0.2) to (0.3, 0.6). Additionally, the words being pronounced by the speaker in each column are highlighted in red.

Anatomically-aware facial animation from a single image. In *ECCV*, 2018. 2, 3

[53] James A Russell. A circumplex model of affect. *Journal of personality and social psychology*, 1980. 1, 2

[54] Shuai Shen, Wanhua Li, Zheng Zhu, Yueqi Duan, Jie Zhou, and Jiwen Lu. Learning dynamic facial radiance fields for few-shot talking head synthesis. In *ECCV*, 2022. 2, 3

[55] Yujun Shen, Jinjin Gu, Xiaoou Tang, and Bolei Zhou. Interpreting the latent space of gans for semantic face editing. In *CVPR*, 2020. 3

[56] Jiaming Song, Chenlin Meng, and Stefano Ermon. Denoising diffusion implicit models. *arXiv:2010.02502*, 2020. 3

[57] Yang Song, Jingwen Zhu, Dawei Li, Xiaolong Wang, and Hairong Qi. Talking face generation by conditional recurrent adversarial network. *arXiv:1804.04786*, 2018. 3

[58] Supasorn Suwajanakorn, Steven M Seitz, and Ira Kemelmacher-Shlizerman. Synthesizing obama: learning lip sync from audio. *ACM Transactions on Graphics (TOG)*, 2017. 6

[59] Jiaxiang Tang, Kaisiyuan Wang, Hang Zhou, Xiaokang Chen, Dongliang He, Tianshu Hu, Jingtuo Liu, Gang Zeng, and Jingdong Wang. Real-time neural radiance talking portrait synthesis via audio-spatial decomposition. *arXiv:2211.12368*, 2022. 2

[60] Jiaxiang Tang, Kaisiyuan Wang, Hang Zhou, Xiaokang Chen, Dongliang He, Tianshu Hu, Jingtuo Liu, Gang Zeng, and Jingdong Wang. Real-time neural radiance talking portrait synthesis via audio-spatial decomposition. *arXiv:2211.12368*, 2022. 3

[61] Antoine Toisoul, Jean Kossaifi, Adrian Bulat, Georgios Tzimiropoulos, and Maja Pantic. Estimation of continuous valence and arousal levels from faces in naturalistic conditions. *Nature Machine Intelligence*, 2021. 7, 1, 2, 6

[62] Omer Tov, Yuval Alaluf, Yotam Nitzan, Or Patashnik, and Daniel Cohen-Or. Designing an encoder for stylegan image manipulation. *ACM Transactions on Graphics (TOG)*, 2021. 1

[63] Duomin Wang, Yu Deng, Zixin Yin, Heung-Yeung Shum, and Baoyuan Wang. Progressive disentangled representation learning for fine-grained controllable talking head synthesis. In *CVPR*, 2023. 3, 6

[64] Suzhen Wang, Lincheng Li, Yu Ding, Changjie Fan, and Xin Yu. Audio2head: Audio-driven one-shot talking-head generation with natural head motion. *arXiv:2107.09293*, 2021. 3

[65] Suzhen Wang, Lincheng Li, Yu Ding, and Xin Yu. One-shot talking face generation from single-speaker audio-visual correlation learning. In *AAAI*, 2022. 3

[66] Zhou Wang, Alan C Bovik, Hamid R Sheikh, and Eero P Simoncelli. Image quality assessment: from error visibility to structural similarity. *IEEE transactions on image processing*, 2004. 6

- [67] Zhenhui Ye, Ziyue Jiang, Yi Ren, Jinglin Liu, Jinzheng He, and Zhou Zhao. Geneface: Generalized and high-fidelity audio-driven 3d talking face synthesis. In *ICLR*, 2023. 2, 3, 6
- [68] Changqian Yu, Jingbo Wang, Chao Peng, Changxin Gao, Gang Yu, and Nong Sang. Bisenet: Bilateral segmentation network for real-time semantic segmentation. In *ECCV*, 2018. 3, 4
- [69] Hongyun Yu, Zhan Qu, Qihang Yu, Jianchuan Chen, Zhonghua Jiang, Zhiwen Chen, Shengyu Zhang, Jimin Xu, Fei Wu, Chengfei Lv, et al. Gaussiantalker: Speaker-specific talking head synthesis via 3d gaussian splatting. *arXiv:2404.14037*, 2024. 2
- [70] Egor Zakharov, Aliaksandra Shysheya, Egor Burkov, and Victor Lempitsky. Few-shot adversarial learning of realistic neural talking head models. In *ICCV*, 2019. 3
- [71] Lvmin Zhang, Anyi Rao, and Maneesh Agrawala. Adding conditional control to text-to-image diffusion models. In *ICCV*, 2023. 7
- [72] Richard Zhang, Phillip Isola, Alexei A Efros, Eli Shechtman, and Oliver Wang. The unreasonable effectiveness of deep features as a perceptual metric. In *CVPR*, 2018. 6
- [73] Zhimeng Zhang, Zhipeng Hu, Wenjin Deng, Changjie Fan, Tangjie Lv, and Yu Ding. Dinet: Deformation inpainting network for realistic face visually dubbing on high resolution video. In *AAAI*, 2023. 3
- [74] Weizhi Zhong, Chaowei Fang, Yinqi Cai, Pengxu Wei, Gangming Zhao, Liang Lin, and Guanbin Li. Identity-preserving talking face generation with landmark and appearance priors. In *CVPR*, 2023. 3
- [75] Hang Zhou, Yu Liu, Ziwei Liu, Ping Luo, and Xiaogang Wang. Talking face generation by adversarially disentangled audio-visual representation. In *AAAI*, 2019. 3
- [76] Hongyu Zhou, Jiahao Shao, Lu Xu, Dongfeng Bai, Weichao Qiu, Bingbing Liu, Yue Wang, Andreas Geiger, and Yiyi Liao. Hugs: Holistic urban 3d scene understanding via gaussian splatting. In *CVPR*, 2024. 2
- [77] Yang Zhou, Xintong Han, Eli Shechtman, Jose Echevarria, Evangelos Kalogerakis, and Dingzeyu Li. Makelttalk: speaker-aware talking-head animation. *ACM Transactions On Graphics (TOG)*, 2020. 3